

~~CONFIDENTIAL~~

19 DEC 1957
13901
14116

TECH LIBRARY KAFB, NM
0149480

NACA RM A57I30

6522



RESEARCH MEMORANDUM

THE EFFECTS OF BOUNDARY-LAYER SEPARATION OVER BODIES OF
REVOLUTION WITH CONICAL TAIL FLARES

By David H. Dennis

Ames Aeronautical Laboratory
Moffett Field, Calif.

Classification of this report (or change to *Unclassified*)
By Authority of *NASA Tech Pub Announcement #25*
(OFFICER AUTHORIZED TO CHANGE)

By *DK* *11 May 61*
NAME AND

AK
GRADE OF OFFICER MAKING CHANGE)

15 May 61
DATE

NATIONAL ADVISORY COMMITTEE
FOR AERONAUTICS

WASHINGTON
December 12, 1957

~~CONFIDENTIAL~~



NATIONAL ADVISORY COMMITTEE FOR AERONAUTICS

RESEARCH MEMORANDUMTHE EFFECTS OF BOUNDARY-LAYER SEPARATION OVER BODIES OF
REVOLUTION WITH CONICAL TAIL FLARES

By David H. Dennis

SUMMARY

Tests were conducted at Mach numbers from 3.0 to 6.3 on bodies of revolution with cone-frustum tail flares to determine the effects on body aerodynamic characteristics of boundary-layer separation in the region of the body-cone-frustum juncture. It was found that laminar separation results in increased normal-force-curve slopes, decreased drags, and large rearward movements of centers of pressure. The forces and moments are considerably more influenced by variations of Mach number and Reynolds number than in the case of no separation.

Theoretical methods for predicting the aerodynamic characteristics for bodies with separation were found to be adequate only if the extents and approximate shapes of the separated flow regions over the bodies were known. For the cases of little or no separation, available inviscid theoretical methods are adequate for estimating the normal-force-curve slope and the center of pressure at zero angle of attack.

INTRODUCTION

Separation of the boundary layers and the resultant effects on the pressures over aircraft surfaces can be an important factor affecting the aerodynamic characteristics of airplanes and missiles. The effects of flow separation are particularly important to the effectiveness and the hinge moments of control surfaces but can also become important to the total aerodynamic forces and moments on aircraft, as was shown for one missile-type configuration in reference 1.

Because theoretical methods for the treatment of boundary-layer separation problems are, at present, inadequate, it is necessary to resort to experimental methods for determining the characteristics and for evaluating the effects of flow separation. For two-dimensional flows, detailed studies encompassing a wide range of flow parameters and

configurations subject to flow separation have recently been reported in reference 2. For three-dimensional flows, however, relatively few data are available from such systematic studies of the problem. The purpose of the present paper is to provide the results of tests to determine the effects of separation on one series of axially symmetric bodies designed to have varying degrees of boundary-layer flow separation at the available test conditions. The body shapes chosen consist of nose sections, a cylindrical midsection, and constant-length cone-frustum tail flares of varying cone angle. The test configurations are also of practical interest in themselves since, for the small flare angles, they might be used as statically stable finless missiles and for the large flare angles as high-drag ballistic-missile re-entry shapes, as suggested in reference 3.

NOTATION

C_D	body foredrag coefficient
C_L	forebody lift coefficient
C_N	body normal-force coefficient
$C_{N\alpha}$	rate of change of normal-force coefficient with angle of attack at $\alpha = 0$, per deg
C_p	pressure coefficient
M_∞	free-stream Mach number
Re	Reynolds number based on body cylinder diameter
x	body axial station measured from nose
\bar{x}	center-of-pressure position, body cylinder diameters aft of nose
α	angle of attack, deg

APPARATUS AND TESTS

The tests were conducted in the Ames 10- by 14-inch supersonic wind tunnel at Mach numbers from 3.0 to 6.3. For a detailed description of the wind tunnel and its flow characteristics see reference 4. The addition, since the publication of reference 4, of a second stage of compression for the supply air permits operation of the wind tunnel at $M_\infty = 5.0$ and 6.3 to higher Reynolds numbers than reported in reference 4. Test

Mach numbers and the corresponding Reynolds numbers based on the diameter of the cylindrical portions of the test bodies (1 in.) were:

M_∞	Re , million
3.00	0.72
4.24	0.62
5.05	0.33 to 0.75
6.28	0.13 to 0.30

For convenience, the test Mach numbers are listed throughout the remainder of this paper as 3.0, 4.2, 5.0, and 6.3.

Each of the 12 models tested consisted of a nose section - a fineness ratio 1.2 cone ($22\text{-}1/2^\circ$ semiapex angle), a fineness ratio 3 cone (9.46° semiapex angle), or a fineness ratio 3 tangent ogive; a 4-diameter long cylindrical midsection; and a cone-frustum tail flare approximately 2.4 cylinder diameters long. The semiangles and the lengths of the tail flares were:

Tail-flare half-angle, deg	Tail-flare length, in.
5.0	2.43
10.5	2.29
15.0	2.40
20.0	2.40

Both pressure-distribution and force tests were conducted for the model having the fineness ratio 1.2 conical nose, 4-diameter-long cylinder, and 20° tail flare. Pressure distributions over the surface of the model were measured at angles of attack to 5° . Data were obtained at each of 15 longitudinal stations. A sketch of the model indicating the location of the orifices is shown in figure 1. The pressures were measured on mercury and on dibutylthalate manometers. Lift, drag, and centers of pressure were determined up to angles of attack of 13° by means of a three-component strain-gage balance. For these tests the measured base pressures were corrected to stream static pressure so that the drag coefficients reported are measures of only the body foredrag.

To evaluate the effects of variations of nose shape and of tail-flare angle, normal forces and pitching moments only, acting on all 12 models, were determined with a strain-gage balance which consisted of a model support sting on which moments were measured at four points. From these four measurements, normal forces, normal-force-curve slopes, and centers of pressure were calculated and checked. Measurements were made at angles of attack from -2° to $+4^\circ$. Test Reynolds numbers for these tests were the lowest of those listed in the preceding table at $M_\infty = 5.0$ and 6.3 .

Wind-tunnel calibration data (see ref. 4) were employed in combination with stagnation pressure measurements to obtain stream static and dynamic pressures.

The accuracy of the test results was influenced by uncertainties in the values of stream dynamic and static pressures and the measurements of the various forces, moments, pressures, and the angles of attack. The estimated maximum errors in the test results caused by these uncertainties are shown in the following table:

	$M_{\infty} = 3.0, 4.2$	$M_{\infty} = 5.0$	$M_{\infty} = 6.3$
C_N, C_L	± 0.01	± 0.02	± 0.04
$C_{N\alpha}$.003	.003	.004
\bar{x}	.2	.2	.4
C_D	.02	.02	.04
C_p	.003	.004	.007
α	$.1^\circ$	$.1^\circ$	$.1^\circ$

Stream Mach numbers in the region of the test body did not vary more than ± 0.03 from the mean values at Mach numbers up to 5.0. A maximum variation of ± 0.05 existed at the highest test Mach number of 6.3.

DISCUSSION OF RESULTS

In the following presentation visual evidence of the flow separation over one of the test bodies is first shown. The effects of the separation on the pressure distributions over the same body and on the gross static aerodynamic characteristics of the body are next shown. The effects of changes in body nose shape and size of tail flares are then discussed relative to the stability and normal-force characteristics of the test bodies at small angles of attack. Finally a short discussion is presented on the adequacy of some theoretical methods available for use in predicting aerodynamic characteristics of axially symmetric bodies with tail flares.

Spark shadowgraph photographs of the flow about the test body having the fineness ratio 1.2 conical nose and largest tail flare (20° half-angle cone frustum) at angles of attack of 0° and 2° are shown in figure 2.¹ It may be seen that changing Mach number and Reynolds number has a profound influence on the flow over the body at $\alpha = 0^\circ$; that is, for flows at low Mach numbers and high Reynolds numbers, the boundary layers are primarily turbulent and little or no separation exists near the cylinder-frustum juncture, while for flows at high Mach numbers and low Reynolds

¹The horizontal streaks in the upper upstream portions of the photographs at $M_{\infty} = 5.0$ and 6.3 result from small quantities of oil on the wind-tunnel windows and are not related to the air flow about the body.

numbers, the boundary layers are, for the most part, laminar and large regions of separation exist. These observations are consistent with those reported for two-dimensional flows in reference 2 where separation phenomena and the effects thereof were classified as to the type of boundary-layer flow over the separated region; that is, (1) boundary layer completely turbulent with little or no separation as in the present tests at $M_{\infty} = 3.0$ (fig. 2(a)); (2) laminar separation with transition occurring in the separated region and turbulent reattachment as at $M_{\infty} = 5.0$ (fig. 2(e)); (3) completely laminar boundary layer to and beyond the reattachment point as at $M_{\infty} = 6.3$ (fig. 2(g)). If any separation exists at $\alpha = 0^{\circ}$ changes of angle of attack from zero result in a decrease in the extent of separation on the windward side of the body and, generally, an increase in the extent of separation on the leeward side.

The same general characteristics as those discussed above were also shown in shadowgraph photographs of the flow about other test bodies having more slender noses and smaller tail flares.

It is thus evident that, insofar as the air flow outside the body boundary layer is concerned, the shape of the body, or, more properly, the pressure generating surface, is essentially altered with changing Mach number and Reynolds number and thus with changing type of boundary layer. Furthermore, for flows where the separation is laminar, and therefore covers a relatively large region, the effective shape is further altered and becomes asymmetrical with changes in angle of attack.

The effects of these changes in pressure generating surface shape on the pressure distributions over one of the test bodies are shown in figures 3 and 4 where the variations of pressure coefficient along the body with the fineness ratio 1.2 conical nose and 20° tail flare are shown. In figure 3 the pressure coefficients along the body at zero angle of attack for the four test Mach numbers are plotted. In figure 4 the pressure coefficients along the windward and the leeward sides of the body at angles of attack up to 5° are shown for each test Mach number.

The differences in the pressure distributions along the afterportion of the cylinder and along the tail flare occasioned by the changes in the extent of flow separation are very evident in figure 3. At Mach number 4.2 it is clear that separation extends only a short distance forward from the tail flare along the cylindrical portion of the body. Aft of the cylinder-frustum juncture at Mach numbers 3.0 and 4.2 the pressure coefficient varies between that for a two-dimensional 20° wedge and that for a 20° conical body, as would be expected from inviscid theory. (See ref. 5.) At the high Mach numbers, however, where the boundary layers are laminar and the regions of separation are large, separation extends well forward along the cylinder and rather than a step rise in pressure at the cylinder-frustum juncture as at $M_{\infty} = 3.0$ and 4.2, the pressure rise is, insofar as can be determined from the data, continuous.

The changes in longitudinal pressure-coefficient distributions along the leeward and the windward sides of the body with changing angle of attack (fig. 4) are as would be expected from the photographs of figure 2; that is, the pressure changes over the tail flare indicate that the regions of separation decrease on the windward side of the body and generally increase somewhat on the lee side. It may be seen that the changes in pressure coefficients over the tail flare with changing angle of attack are much larger in the case of extensive flow separation than in the case of little or no separation (cf. figs. 4(d) and 4(a)). This results, of course, from the alteration of the effective body shape with angle of attack, as mentioned previously, and has a profound influence on the variations with angle of attack of the over-all forces and moments acting on the body, as will be discussed later. It is interesting to note that the increase in the size of the region of separation on the lee side of the cylindrical portion of the body and the decrease on the windward side at high Mach numbers are such that the pressures on the cylinder are not appreciably altered by small changes in angle of attack. It was observed from photographs, in fact, that, at least in the pitch plane, the outer edge of the boundary layer over the cylindrical portion of the body retains its alignment with the free stream while the body pitches within the separated flow region.

The total aerodynamic forces (excluding base drag) on the body having the fineness ratio 1.2 conical nose and 20° tail flare are shown in figures 5 and 6. The effects of variations of Mach number and of Reynolds number on the normal force at small angles of attack are shown in figure 5, and the effects on lift, drag, and center-of-pressure position to relatively high angles of attack are shown in figure 6. It may be seen in figure 5 that variations of Mach number and Reynolds number induce large changes in normal-force coefficient at small angles of attack. It can be shown analytically (see e.g., ref. 5) that the normal-force-curve slope (and, therefore, the normal forces at small angles of attack) for the test body is relatively independent of the extent of flow separation so long as the effective pressure generating surface (i.e., the outer surface of the separated flow regions) remains axially symmetric. It is apparent then that the very large changes in normal-force coefficient shown in figure 5 must be attributed, for the most part, to the development of asymmetrical separated flow regions as discussed previously. There exists a relatively large effect of varying Mach number at constant Reynolds number as is evident from comparisons of the corresponding values of C_N for $M_\infty = 6.3$, $Re = 0.30$ million with that for $M_\infty = 5.0$, $Re = 0.33$ million and for $M_\infty = 5.0$, $Re = 0.75$ million with that for $M_\infty = 3.0$, $Re = 0.72$ million. The increase in C_N with Mach number at a fixed Reynolds number occurs because, for laminar flows, the region of separation at the higher Mach numbers is larger. Thus the boundary layer is subject to greater asymmetry with changing angle of attack. The region

of separation is larger, in part, due to the inability of the boundary layer to negotiate the greater pressure rise that would exist at the cylinder-tail-flare juncture at the higher Mach number in the absence of separation.

Tests were also made with boundary-layer trips applied to the nose of the model. The Reynolds numbers at $M_\infty = 5.0$ and 6.3 were 0.33 and 0.13 million, respectively. The method of inducing transition was relatively effective at $M_\infty = 5.0$, the extent of boundary-layer separation being reduced to about the same as that at $M_\infty = 4.2$, $Re = 0.62$ million. At $M_\infty = 6.3$, however, the flow was still laminar at the separation point with transition occurring in the separated region near the point of reattachment to the tail flare. The extent of the separated region was appreciably reduced, however, from that which existed at the same Reynolds number without the nose-tip roughness. The normal-force curves for this test on the fineness ratio 1.2 conical-nose body were very nearly coincident with those shown in figure 5 for the highest test Reynolds numbers ($Re = 0.75$ million at $M_\infty = 5.0$ and $Re = 0.30$ million at $M_\infty = 6.3$). From photographs it was evident that the flow fields about the body also were very similar for the high Reynolds number tests and the lower Reynolds number tests with the boundary-layer trip. The trip did not measurably affect the aerodynamic characteristics of the body at $M_\infty = 3.0$ and had but a slight effect at $M_\infty = 4.2$.

From the test results shown in figure 6 it is evident that, associated with the increase of C_N with increasing Mach number, the drag coefficient decreases and the center of pressure moves aft, particularly for the lower angles of attack. At the high angles the force characteristics do not differ as markedly with changing M_∞ and/or Re since at these angles the flow about the body does not change appreciably; that is, the flow is essentially attached along most of the windward side of the body and fully separated on the lee side regardless of the Mach number and Reynolds number of the flow. The nonlinearities at small angles of attack of the lift and center-of-pressure curves for the flows at high Mach numbers and low Reynolds numbers are due primarily to the decrease in the size of the separated region on the windward side of the body with increasing angle of attack. The large decrease of zero-lift drag coefficient with increasing Mach number and decreasing Reynolds number, although in part due to the expected decrease with increasing M_∞ , is, for the most part, due to the decrease in pressure over the tail flare resulting from the flow separation.

The effects of varying the tail flare angle of the test bodies on the normal-force-curve slopes and on the center-of-pressure positions at zero angle of attack are shown in figures 7 and 8, respectively. The results shown at 0° tail flare angle for the fineness ratio 3 cone and ogive nosed models were obtained from interpolations of test results previously reported in reference 5. The repeatability of these test results is indicated by showing with the results of the present tests the results

of the tests reported in reference 1 for the fineness ratio 1.2 conical nosed body with the 20° tail flare (figs. 7(a) and 8(a)). It should be noted that the reference area for the normal-force coefficients is the cross-sectional area of the cylindrical portion of the bodies. Thus, the values of the normal-force-curve slopes would be expected to increase somewhat with increasing tail flare angle. The increases in $C_{N\alpha}$ with tail flare angle at $M_\infty = 3.0$ and 4.2 are of approximately the same magnitude as those which would be estimated with Newtonian theory while, of course, the increases at $M_\infty = 5.0$ and 6.3 are much greater and are related to the separation phenomena.

It may be seen that, in general, the curves for the bodies having fineness ratio 3 conical noses are very similar to those for bodies having fineness ratio 3 ogival noses (figs. 7(b), 7(c), 8(b), and 8(c)), indicating relatively little effect of profile shape of equal fineness ratio noses on the normal-force and center-of-pressure characteristics. Results for the bodies having the fineness ratio 1.2 conical noses show qualitative agreement with those for the other bodies, but the normal-force-curve slopes are consistently somewhat lower than for the fineness ratio 3 nosed bodies for tail flare angles greater than 5°. For $M_\infty = 3.0$ and 4.2 the differences in $C_{N\alpha}$ may be related approximately to the differences of $C_{N\alpha}$ of the noses alone (see, e.g., ref. 5). However, at $M_\infty = 5.0$ and 6.3 the differences are much larger and are probably related to the differences in the sizes of the regions of separated flow. It would be expected, of course, that the pressure distributions over the forward part of the relatively blunt-nosed models would differ appreciably from those over the more slender bodies, thus altering the extents and shapes of the separated flow regions.

Although there is a marked effect of changing Mach number and Reynolds number from $M_\infty = 5.0$ to 6.3 for the 15° and 20° flare angles, there is little difference in the values of $C_{N\alpha}$ and \bar{x} between $M_\infty = 5.0$ and 6.3 for tail flares of 5° and 10°. The relatively small effects are, in fact, generally the reverse of those that occur for the large flare angles. Study of shadowgraph photographs of the flow about the test bodies revealed that, again, these characteristics are related to the flow separation phenomena; that is, for tail flare angles of 15° and 20° the regions of separation were markedly different at $M_\infty = 5.0$ and 6.3 while they were much the same at the two Mach numbers for the smaller tail flares. For the small flare angles the entire boundary layer to, and somewhat beyond, the reattachment point was laminar at both Mach numbers and the general flow pattern appeared to be much the same. For the large flare angles, transition occurred in the separated boundary layer at $M_\infty = 5.0$ while at $M_\infty = 6.3$ the flow remained laminar over the entire length of the body, and the flow patterns were quite different with a considerably larger separated region at Mach number 6.3 than at $M_\infty = 5.0$. It becomes evident then that, as pointed out in reference 2, the condition of the boundary layer over the separated region - completely laminar, transitional, or fully turbulent - has a profound influence on the extent of separated flow and thus on the local pressure distributions and the over-all aerodynamic characteristics.

CONFIDENTIAL

COMPARISONS WITH THEORY

Theoretical calculations of the normal-force-curve slopes and center-of-pressure positions were made for two of the body shapes tested: the fineness ratio 1.2 conical nosed body with 20° tail flare and the fineness ratio 3 conical nosed body with 10° tail flare. The comparisons of the theoretical results to experimental results are shown in figure 9. Computations were made using the generalized shock-expansion method of reference 6 and the second-order shock-expansion method of reference 5 for the bodies at all of the four test Mach numbers. To include the effects of separation, the second-order method was applied at $M_\infty = 5.0$ and 6.3 and the Newtonian, or impact theory (see, e.g., ref. 7), at $M_\infty = 6.3$ to the body shapes as modified to include the entire separated flow regions. Shadowgraph photographs taken at several angles of attack up to 2° were used to determine the modified body shapes and the normal forces and centers of pressure were calculated at these discrete angles. Curves were faired through the calculated points and the values of C_N at $\alpha = 0$ and \bar{x} at $\alpha = 0$, were determined from the curves. In figure 9 the results of these calculations using the second-order method are shown for simplicity as straight lines between $M_\infty = 5.0$ and 6.3. It should not be inferred, however, that the method predicts such variations of C_N and \bar{x} with changing Mach number since the characteristics were determined at only the above-mentioned discrete points.

As would be expected, agreement of the inviscid theoretical results with experiment is relatively good at the low Mach numbers where there is little flow separation and the agreement is quite poor at the higher Mach numbers where large regions of laminar separation exist. The results of calculations using the "modified" body shapes are in relatively good agreement with the experimental results, however, particularly for the body with the 20° tail flare. It is evident from figure 9 then, that these theories may be used to estimate, at least qualitatively, the effects of flow separation on the aerodynamic characteristics of bodies of revolution, provided that the body configurations as modified by the separation are known.

CONCLUDING REMARKS

It has been found that if appreciable boundary-layer separation occurs over a nose-cylinder cone-frustum body, the stabilizing effect of the cone-frustum tail flare is much greater than that which would be indicated from inviscid theoretical calculations. Also, the normal-force-curve slope at zero angle of attack is greater and the drag is considerably less than would be predicted. Furthermore, relatively small variations in stream Reynolds number and/or Mach number have a profound influence on the character of the boundary layer and thus on the extent

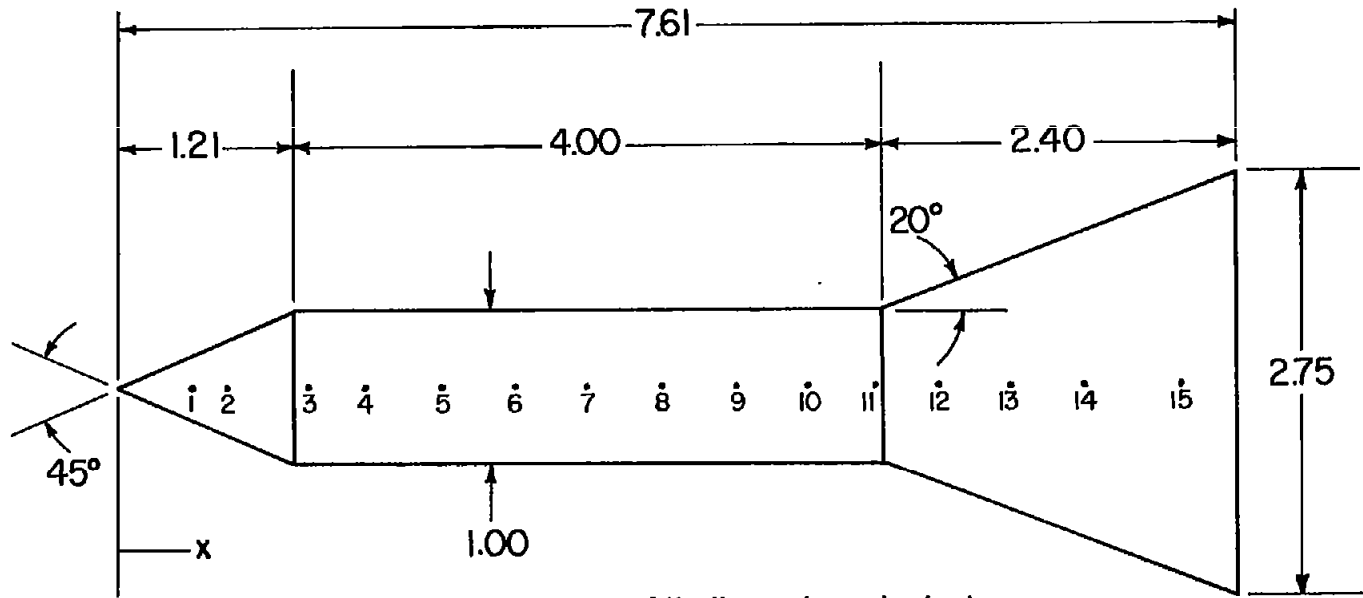
of flow separation. This results in relatively large changes in the local pressure distributions over the bodies and on the over-all aerodynamic characteristics of the bodies. These changes are far greater than those which would occur with corresponding changes in Reynolds number and Mach number in the case of no boundary-layer separation.

Theoretical methods are available for use in predicting relatively accurately the characteristics of bodies having base flares. However, for the flow conditions at which extensive boundary-layer separation occurs, the extent and shape of such separated regions must be known. Unfortunately, to date, no adequate method for estimating the required separation characteristics is available for three-dimensional shapes. Thus recourse must be made either to rather extensive flow visualization studies or to force or pressure distribution tests.

Ames Aeronautical Laboratory
National Advisory Committee for Aeronautics
Moffett Field, Calif., Sept. 30, 1957

REFERENCES

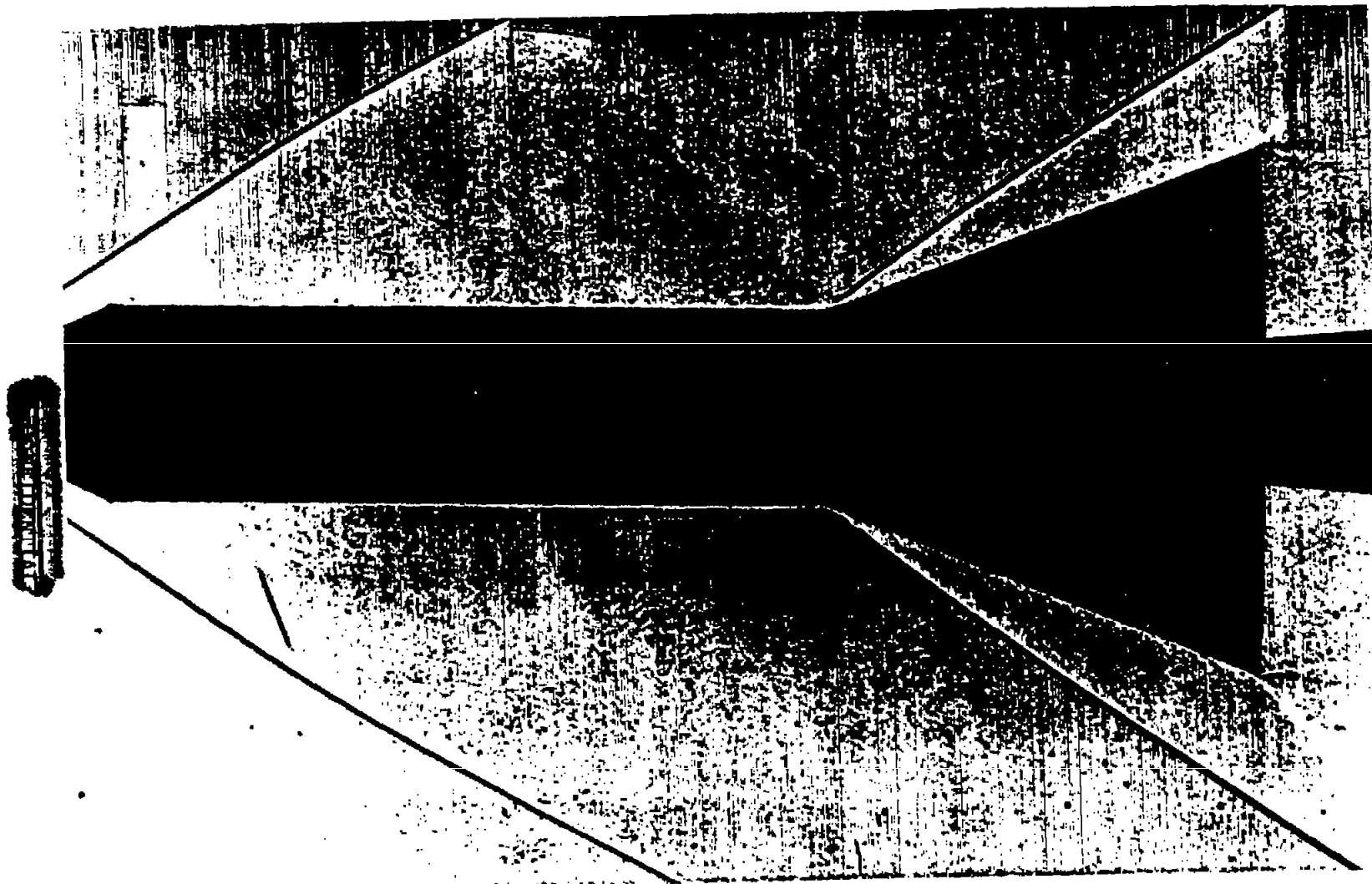
1. Dennis, David H., and Syvertson, Clarence A.: Effects of Boundary-Layer Separation on Normal Force and Center of Pressure of a Cone-Cylinder Model With a Large Base Flare at Mach Numbers From 3.00 to 6.28. NACA RM A55H09, 1955.
2. Chapman, Dean R., Kuehn, Donald M., and Larson, Howard K.: Investigation of Separated Flows in Supersonic and Subsonic Streams With Emphasis on the Effect of Transition. NACA TN 3869, 1957.
3. Allen, H. Julian, and Eggers, A. J., Jr.: A Study of the Motion and Aerodynamic Heating of Missiles Entering the Earth's Atmosphere at High Supersonic Speeds. NACA TN 4047, 1957. (Supersedes NACA RM A53D28)
4. Eggers, A. J., Jr., and Nothwang, George J.: The Ames 10- by 14-Inch Supersonic Wind Tunnel. NACA TN 3095, 1954.
5. Syvertson, Clarence A., and Dennis, David H.: A Second-Order Shock-Expansion Method Applicable to Bodies of Revolution Near Zero Lift. NACA TN 3527, 1956.
6. Eggers, A. J., Jr., and Savin, Raymond C.: A Unified Two-Dimensional Approach to the Calculation of Three-Dimensional Hypersonic Flows, With Application to Bodies of Revolution. NACA Rep. 1249, 1955.
7. Grimminger, G., Williams, E. P., and Young, G. B. W.: Lift on Inclined Bodies of Revolution in Hypersonic Flow. Jour. Aero. Sci., vol. 17, no. 11, Nov. 1950, pp. 675-690.



All dimensions in inches.

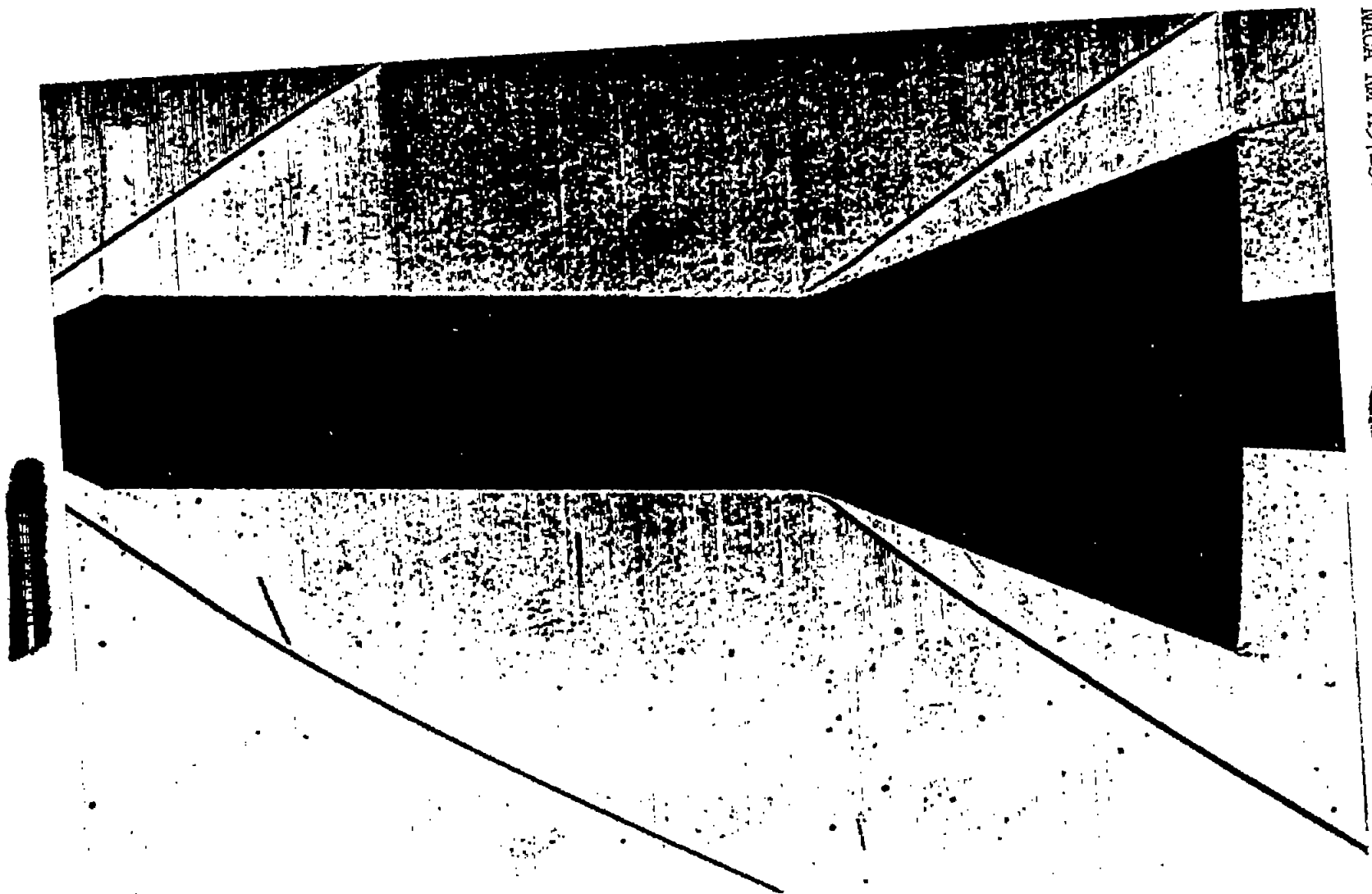
Orifice number	Orifice location, x, inches from body nose	Orifice number	Orifice location, x, inches from body nose
1	.50	8	3.69
2	.75	9	4.19
3	1.31	10	4.69
4	1.69	11	5.15
5	2.19	12	5.58
6	2.69	13	6.08
7	3.19	14	6.58
		15	7.21

Figure 1.- Location of orifices on pressure-distribution model.



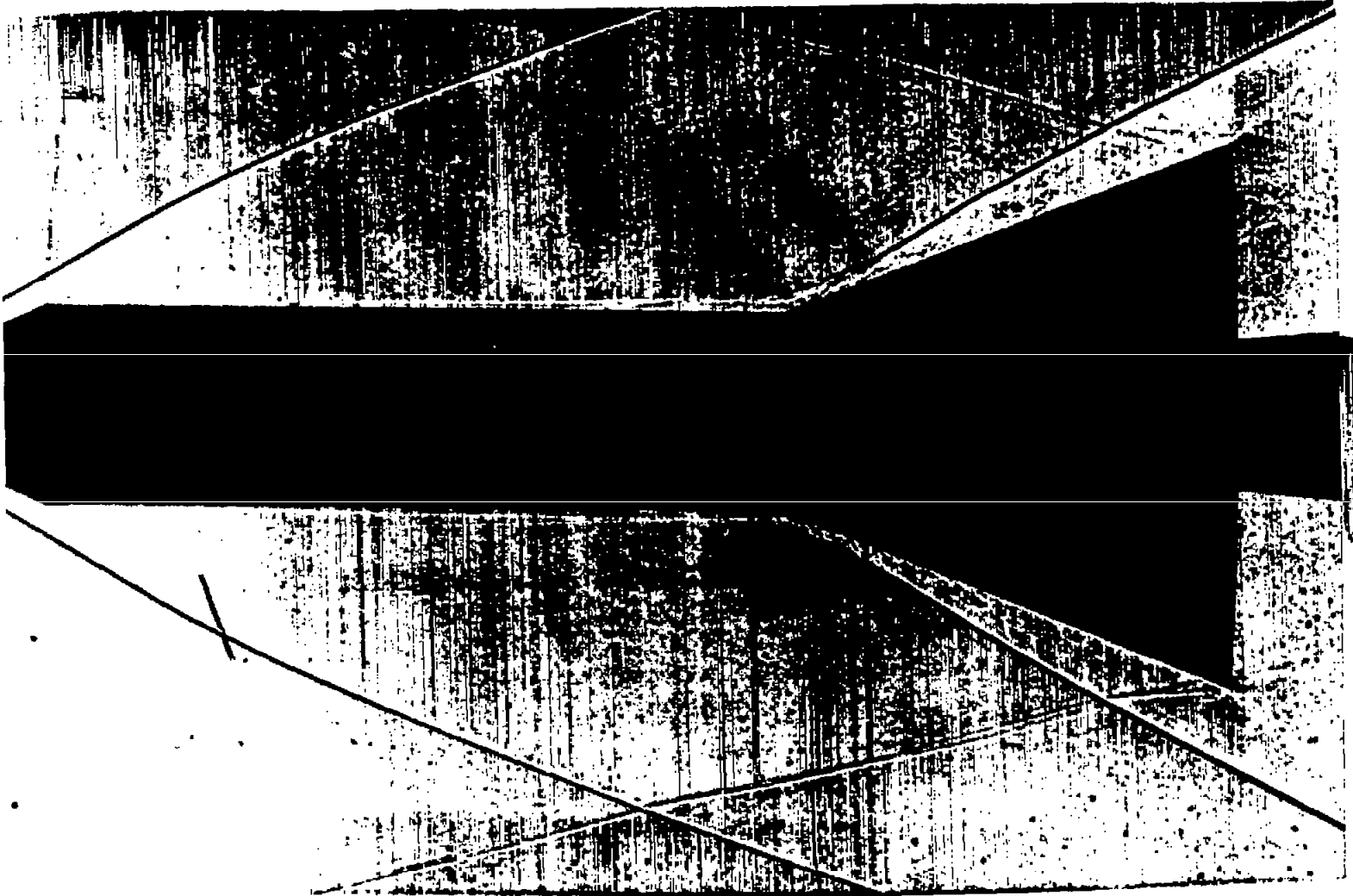
(a) $M_\infty = 3.0$, $Re = 0.72$ million, $\alpha = 0^\circ$, turbulent boundary layer.

Figure 2.- Flow about body with fineness ratio 1.2 conical nose and 20° tail flare.



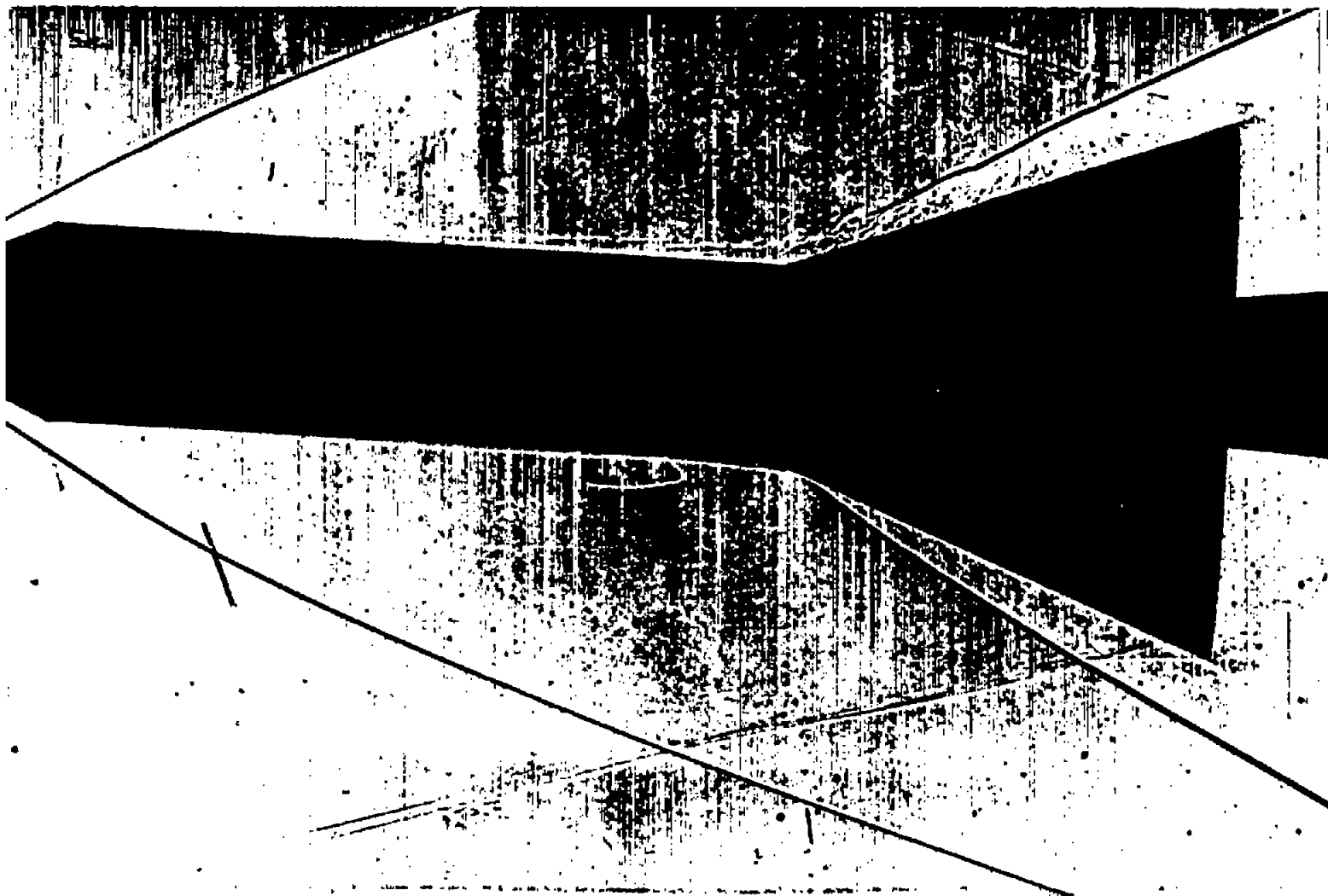
(b) $M_{\infty} = 3.0$, $Re = 0.72$ million, $\alpha = 2^{\circ}$.

Figure 2.- Continued.



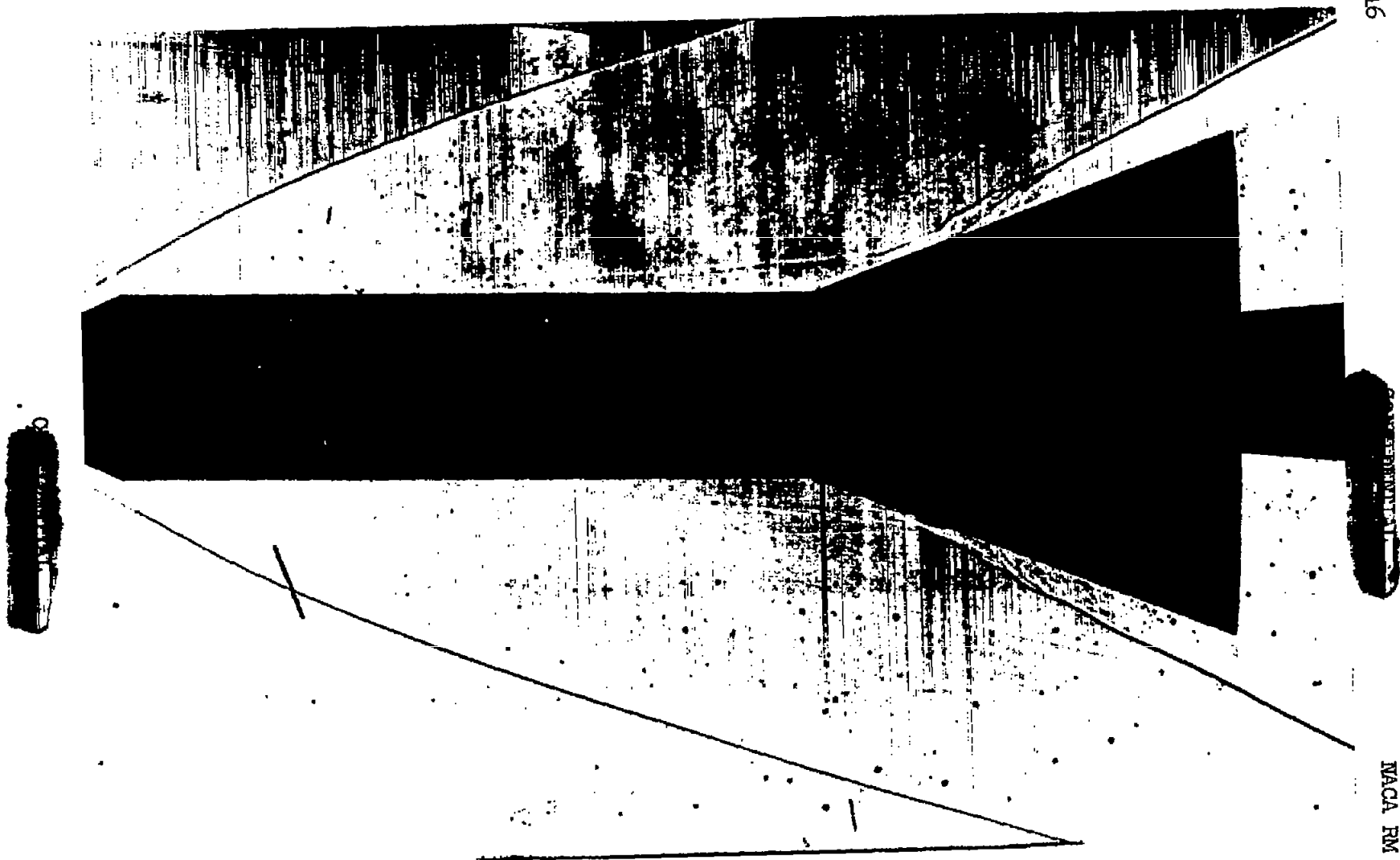
(c) $M_\infty = 4.2$, $Re = 0.62$ million, $\alpha = 0^\circ$, boundary layer transitional at separation.

Figure 2.- Continued.



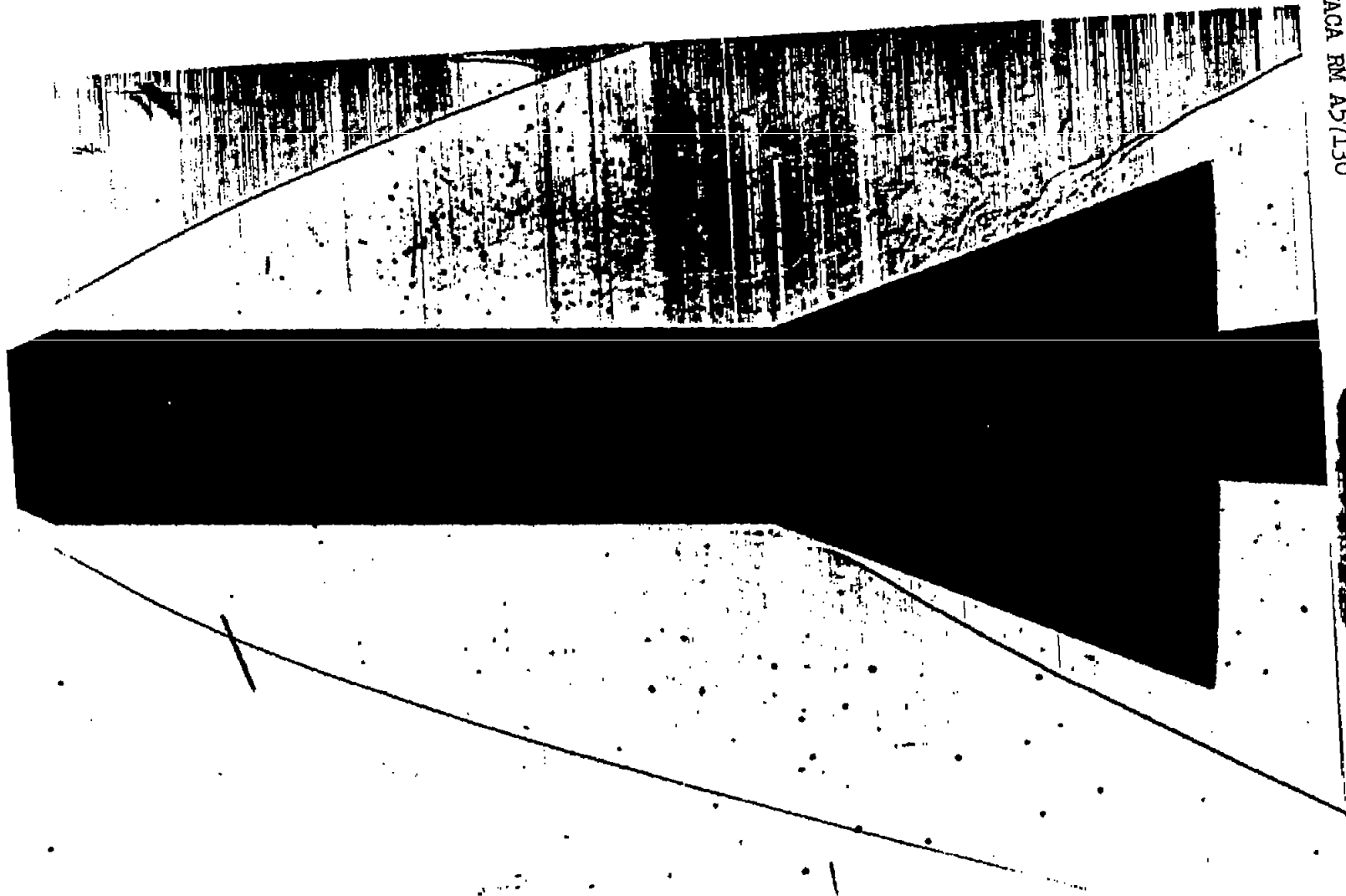
(d) $M_\infty = 4.2$, $Re = 0.62$ million, $\alpha = 2^\circ$.

Figure 2.- Continued.



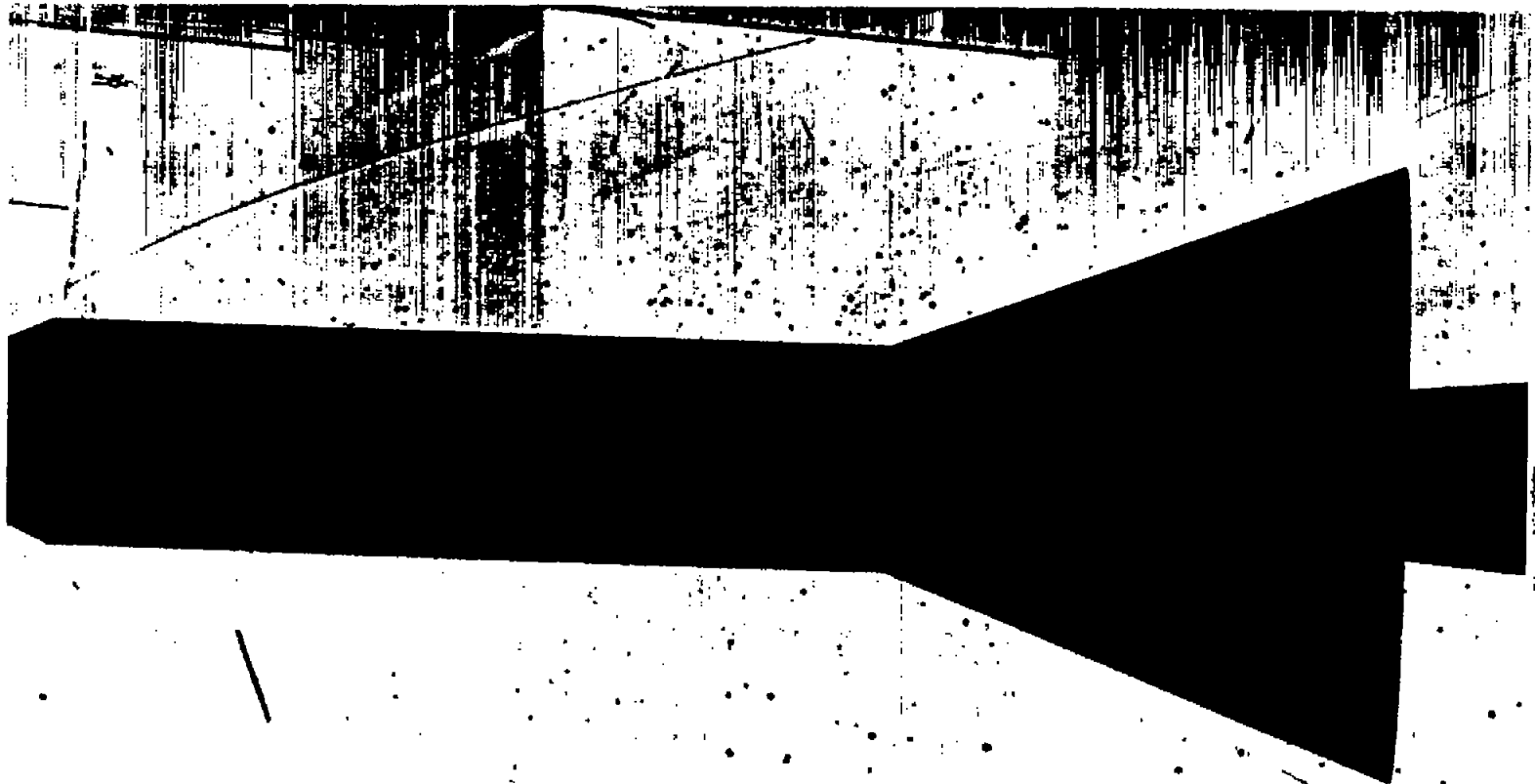
(e) $M_\infty = 5.0$, $Re = 0.33$ million, $\alpha = 0^\circ$, boundary layer laminar at separation.

Figure 2.- Continued.



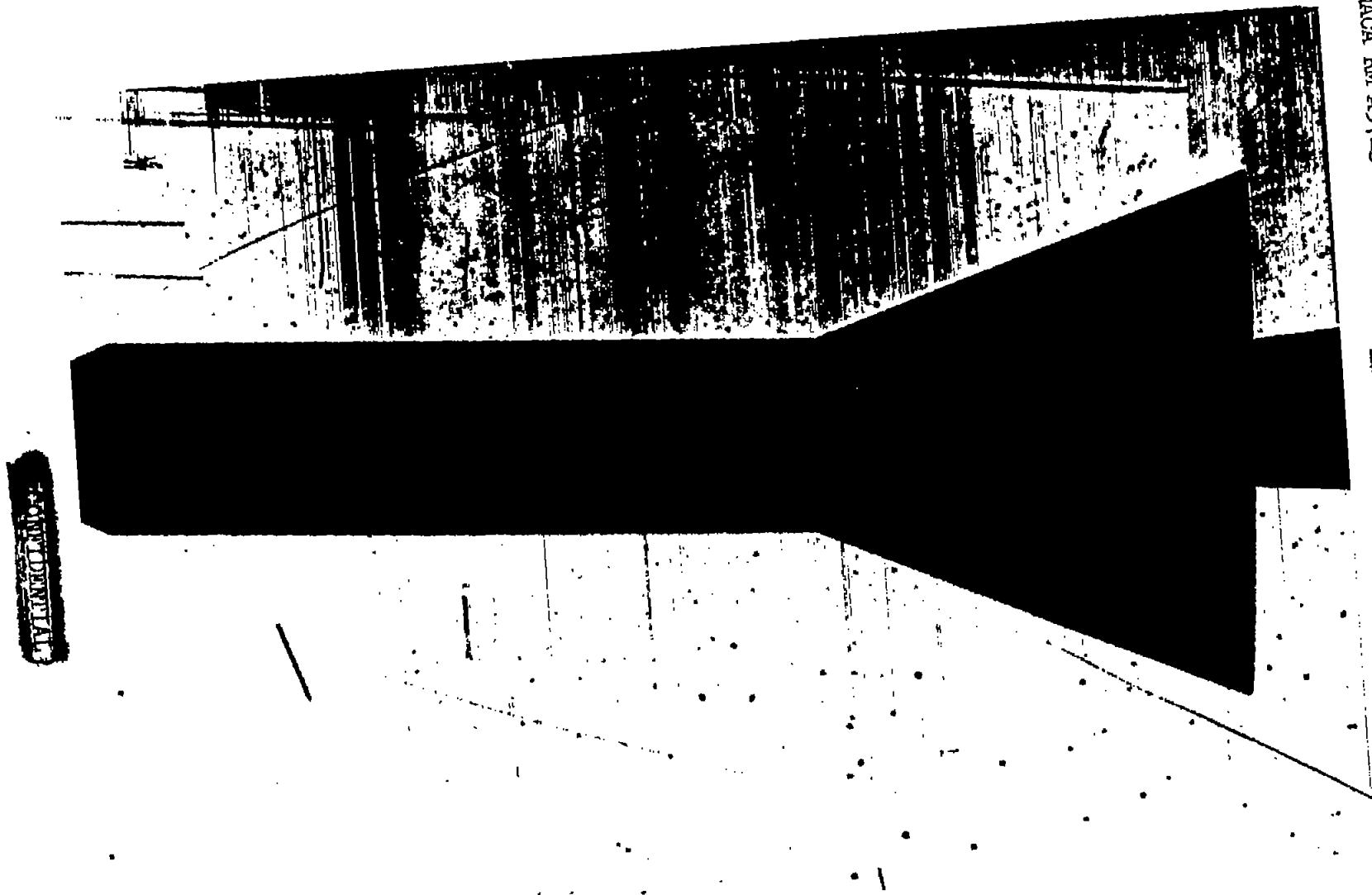
(f) $M_{\infty} = 5.0$, $Re = 0.33$ million, $\alpha = 2^{\circ}$.

Figure 2.- Continued.



(g) $M_{\infty} = 6.3$, $Re = 0.13$ million, $\alpha = 0^{\circ}$, laminar boundary layer.

Figure 2.- Continued.



(h) $M_{\infty} = 6.3$, $Re = 0.13$ million, $\alpha = 2^{\circ}$.
Figure 2.- Concluded.

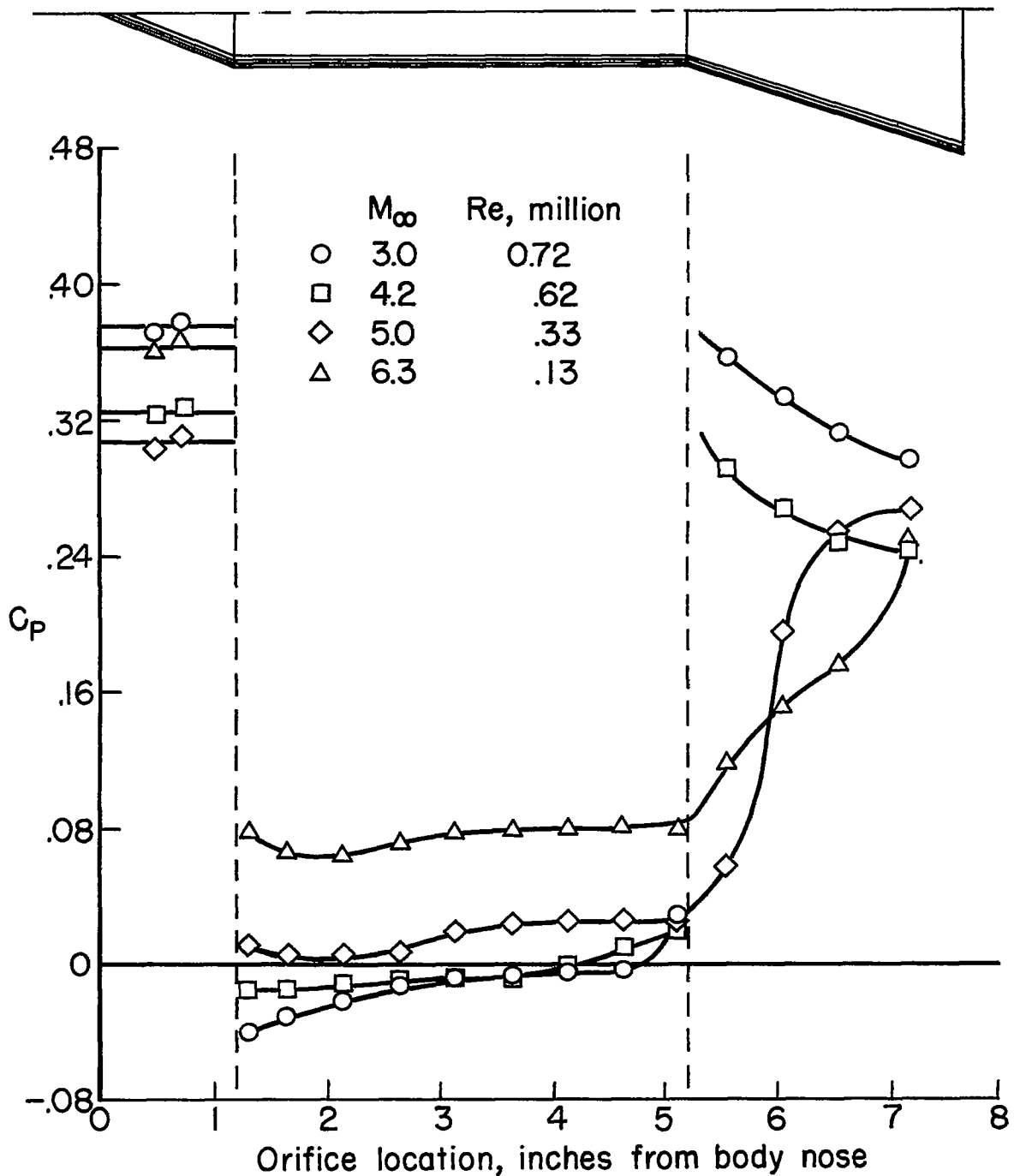
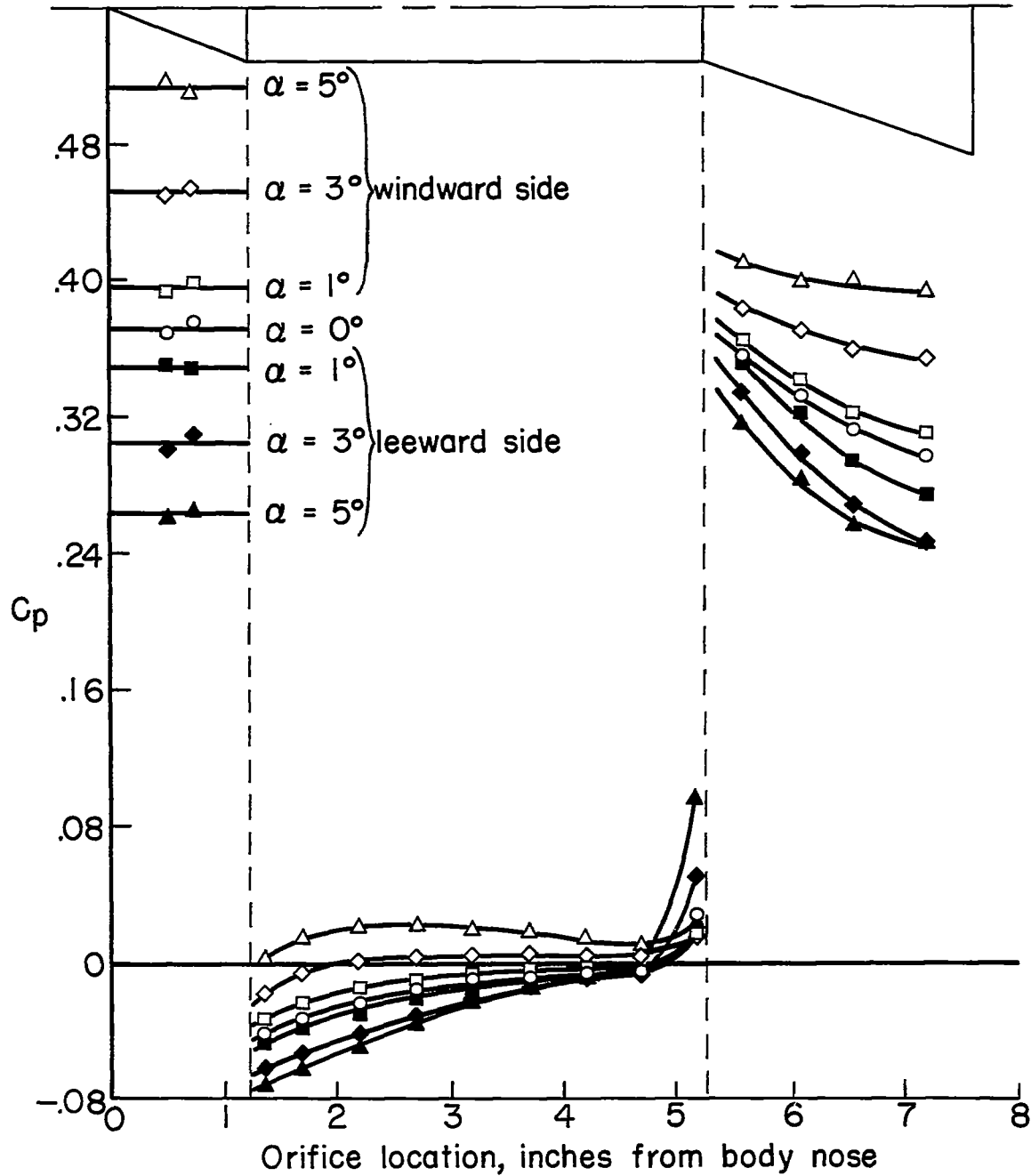


Figure 3.- Longitudinal pressure distributions over the test body with fineness ratio 1.2 conical nose and 20° tail flare ($\alpha = 0^\circ$).



(a) $M_\infty = 3.0$

Figure 4.- Longitudinal pressure distributions for various angles of attack over the test body with fineness ratio 1.2 conical nose and 20° tail flare.

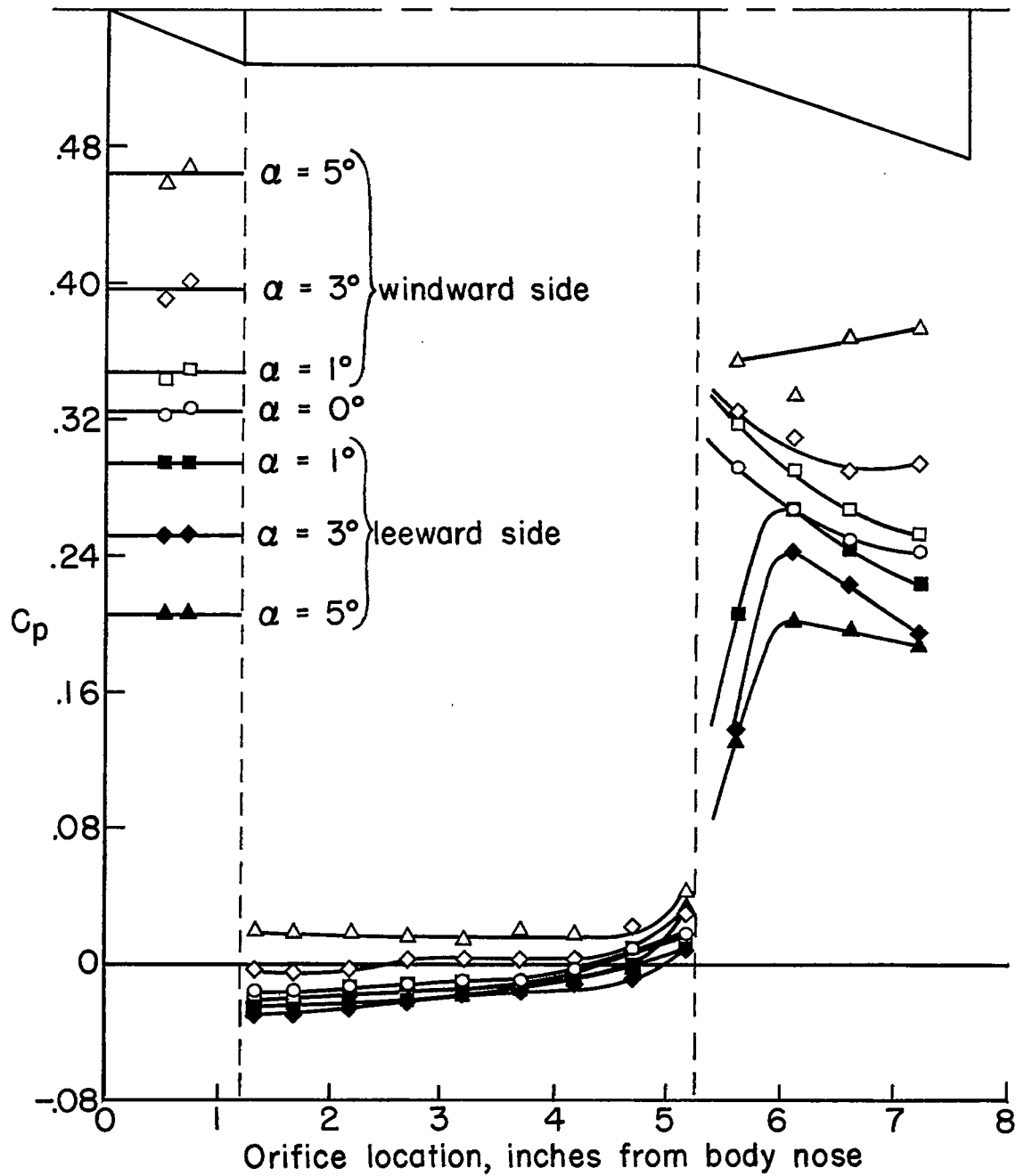
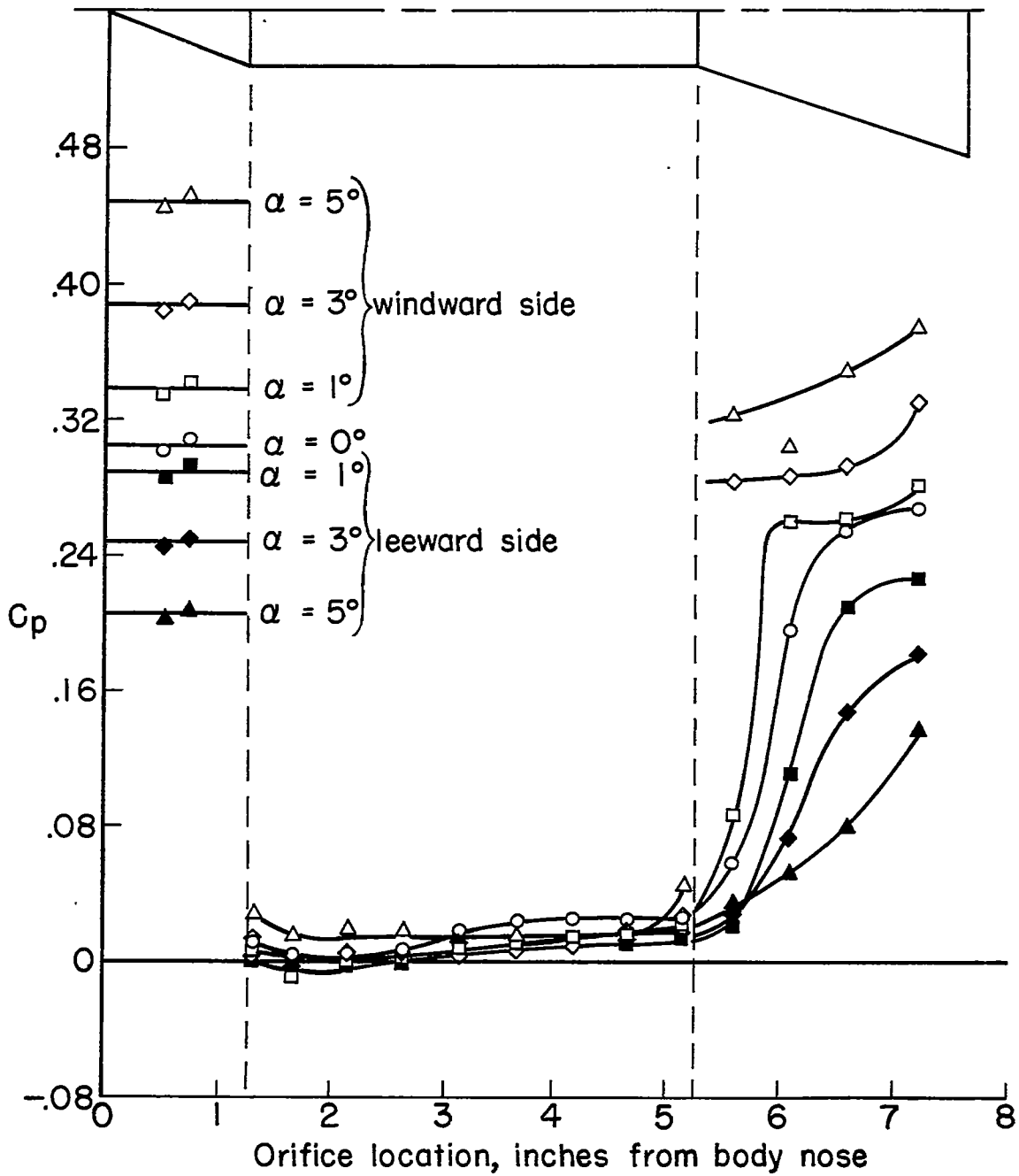
(b) $M_\infty = 4.2$

Figure 4.- Continued.



(c) $M_\infty = 5.0$

Figure 4.- Continued.

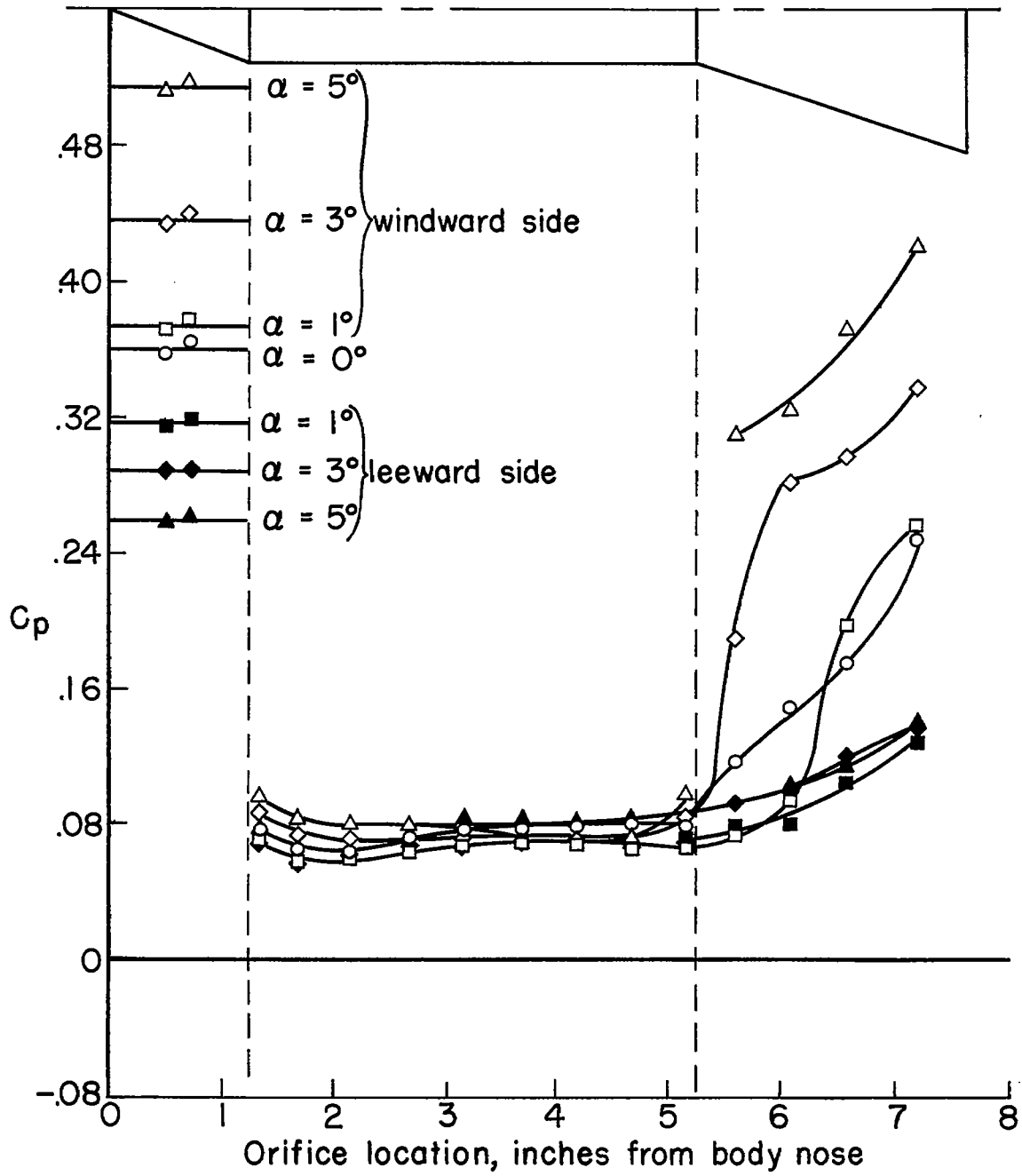
(d) $M_\infty = 6.3$

Figure 4.- Concluded.

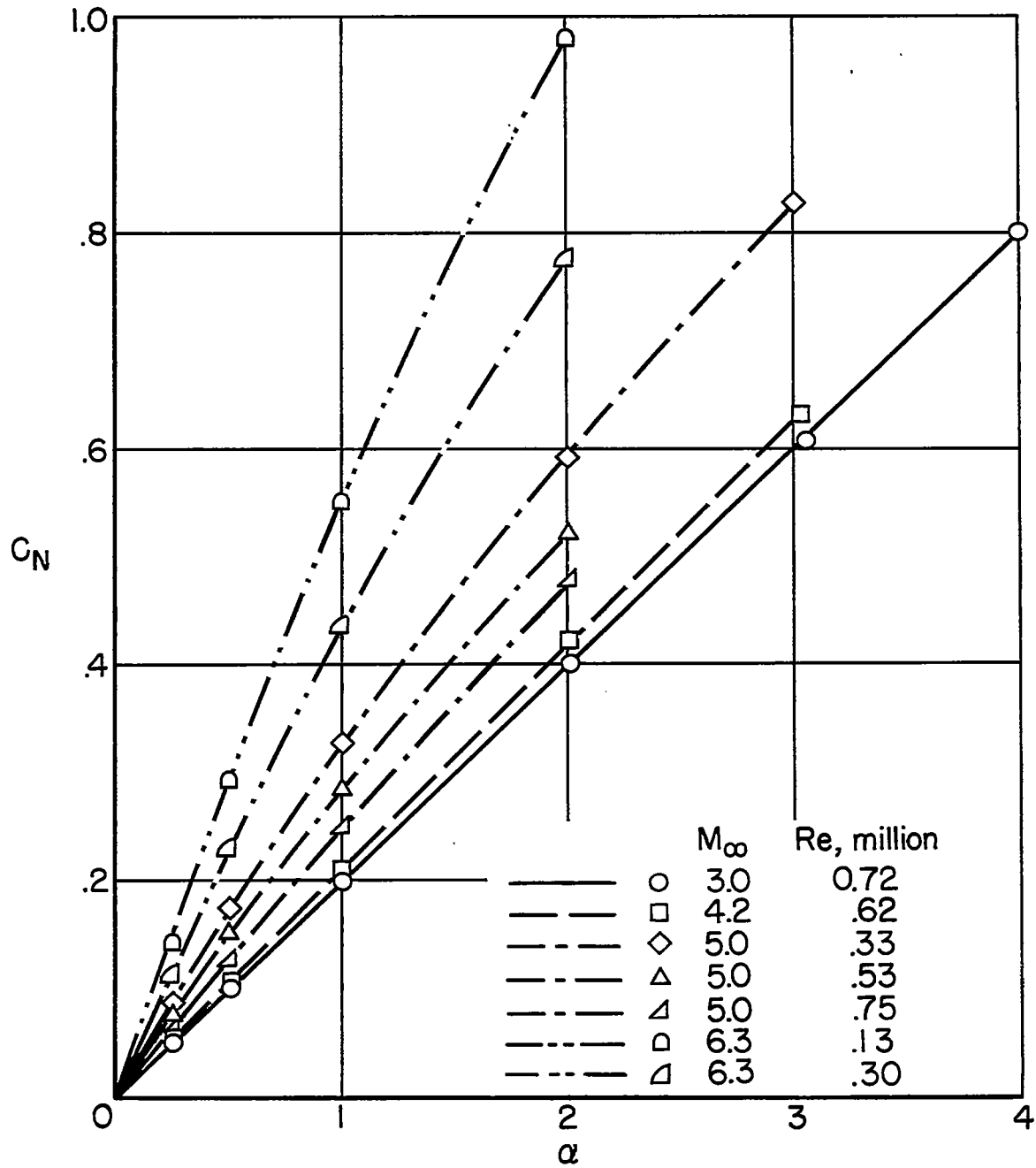


Figure 5.- Normal-force coefficients at small angles of attack on the test body with fineness ratio 1.2 conical nose and 20° tail flare.

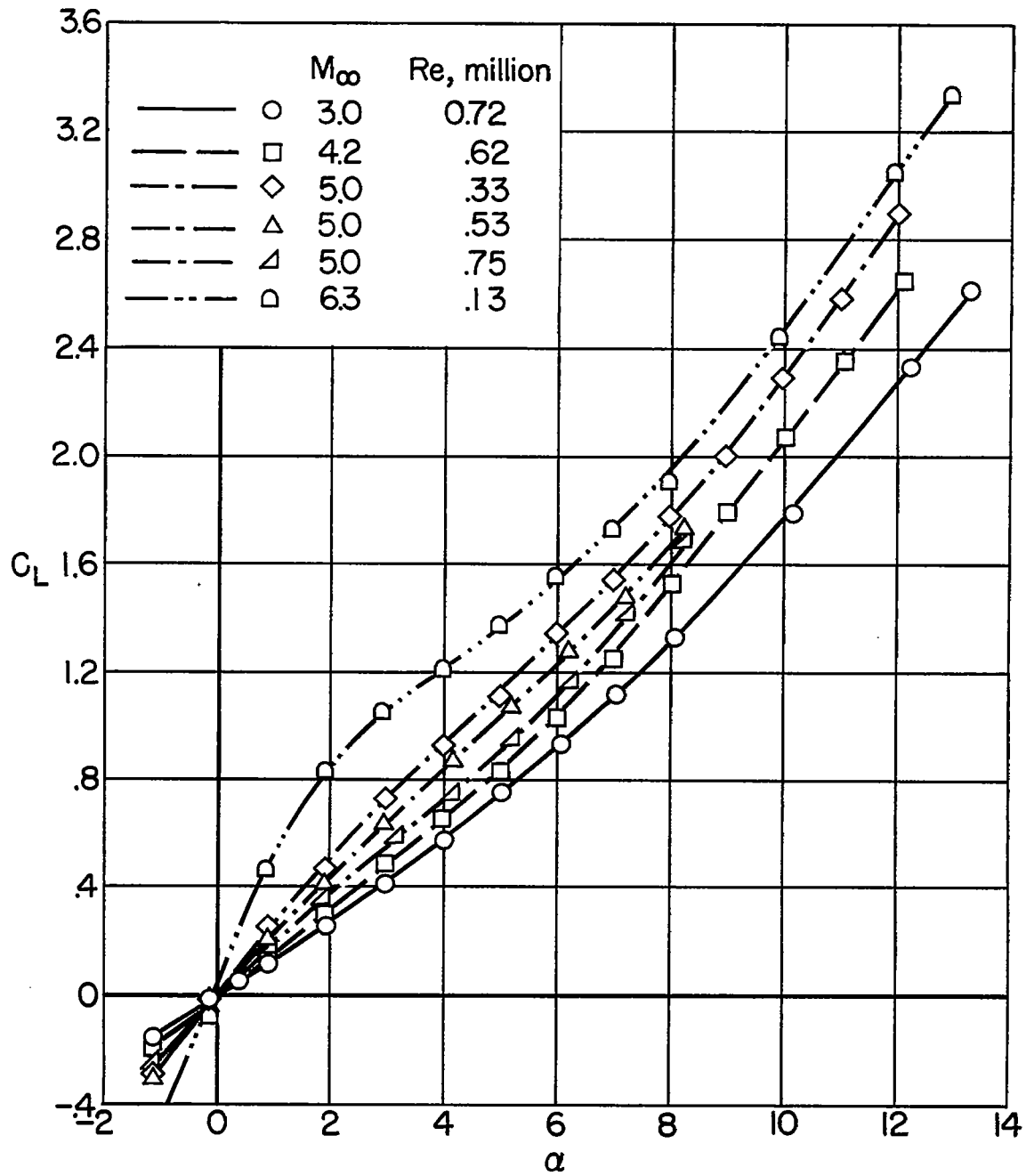
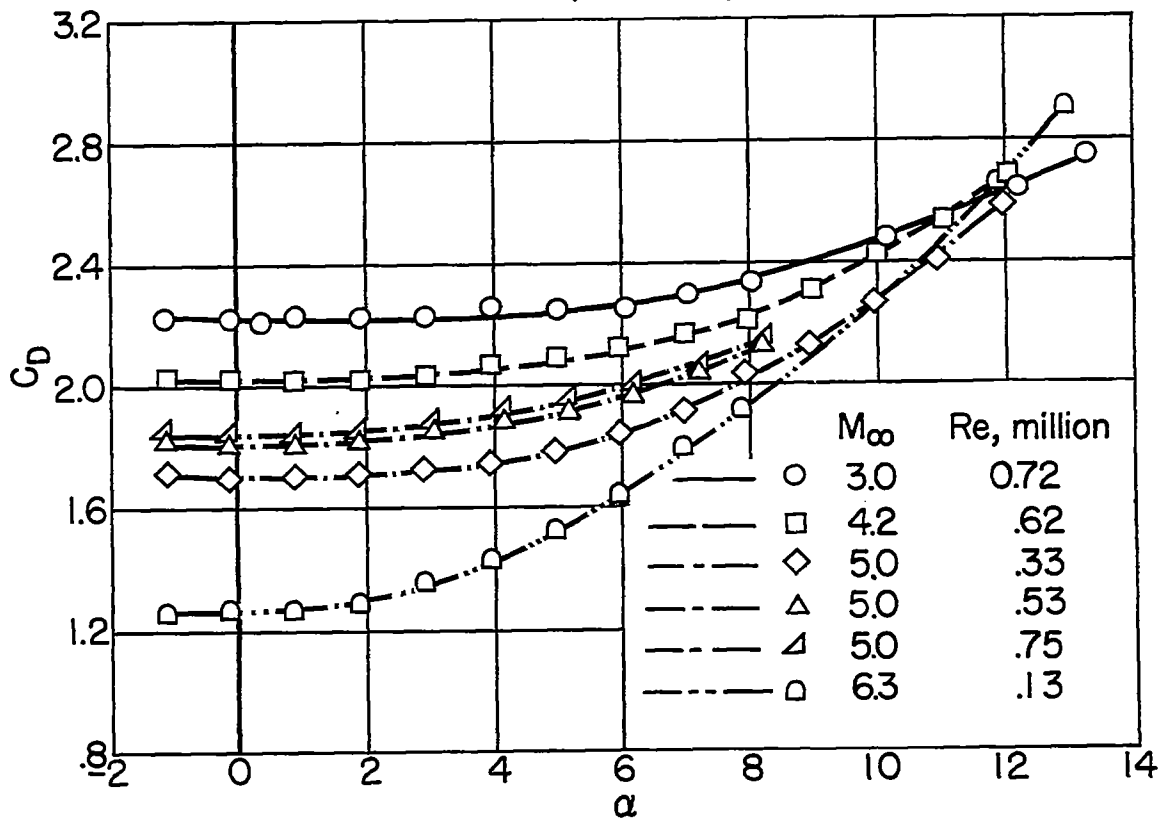
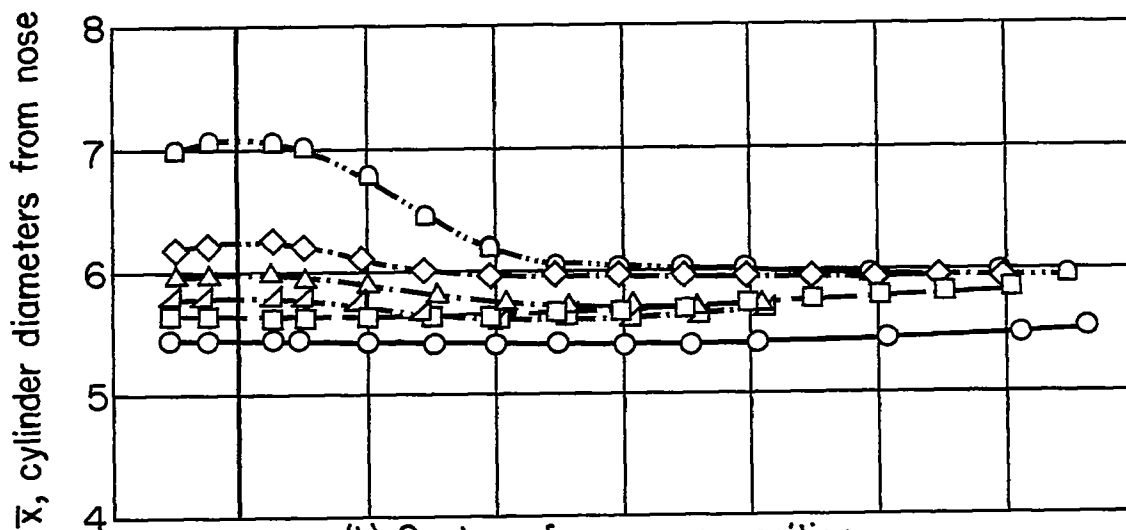
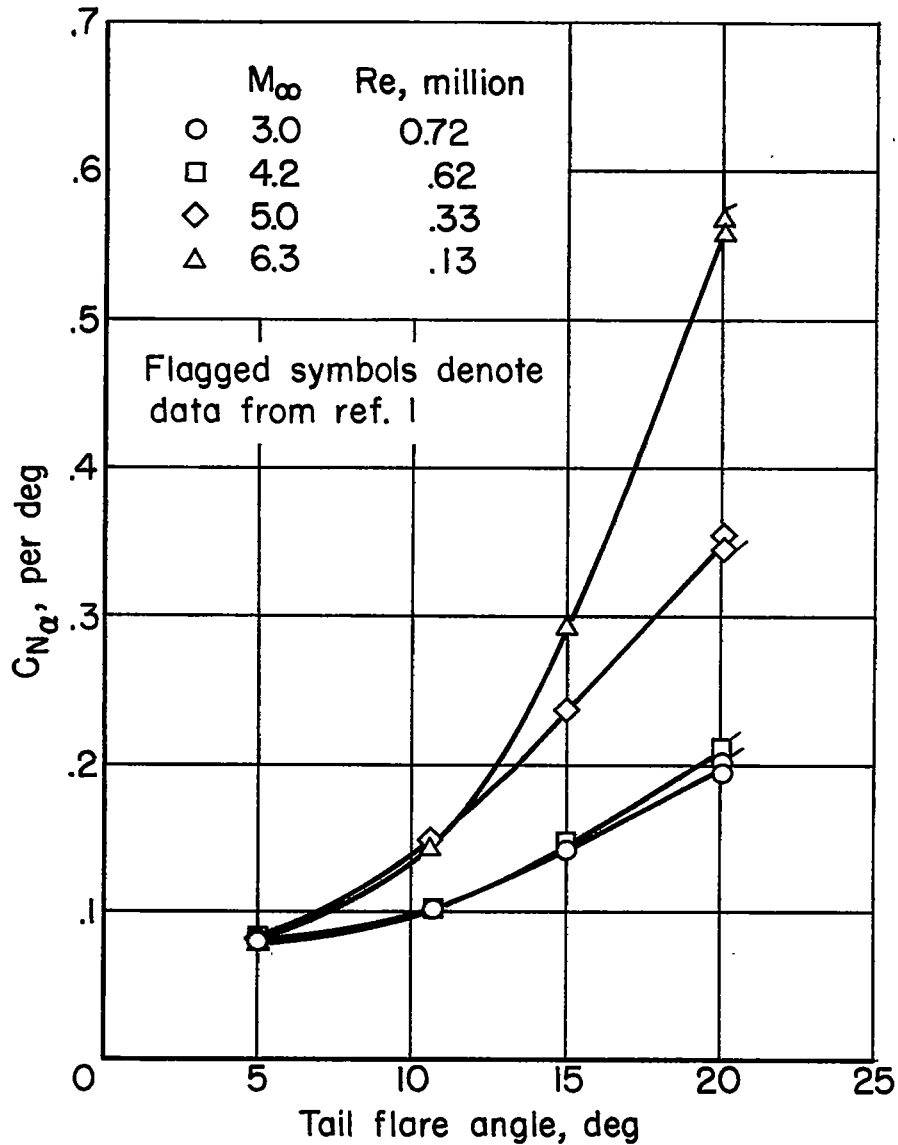
(a) C_L

Figure 6.- Aerodynamic characteristics of the test body with fineness ratio 1.2 conical nose and 20° tail flare angle.



(c) C_D

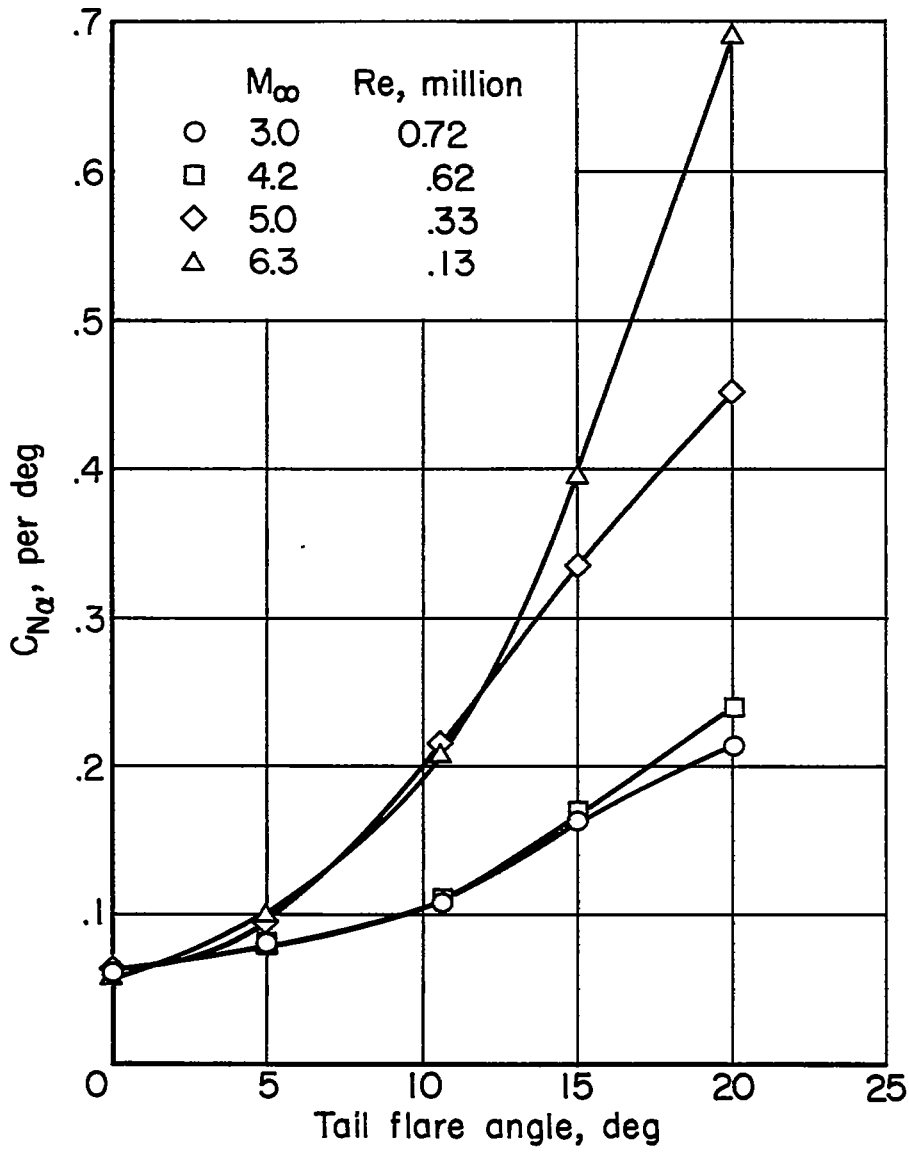
Figure 6.- Concluded.

~~CONFIDENTIAL~~

(a) Bodies with fineness ratio 1.2 conical noses.

Figure 7.- Variations of normal-force-curve slopes with tail flare angle for the 12 test bodies.

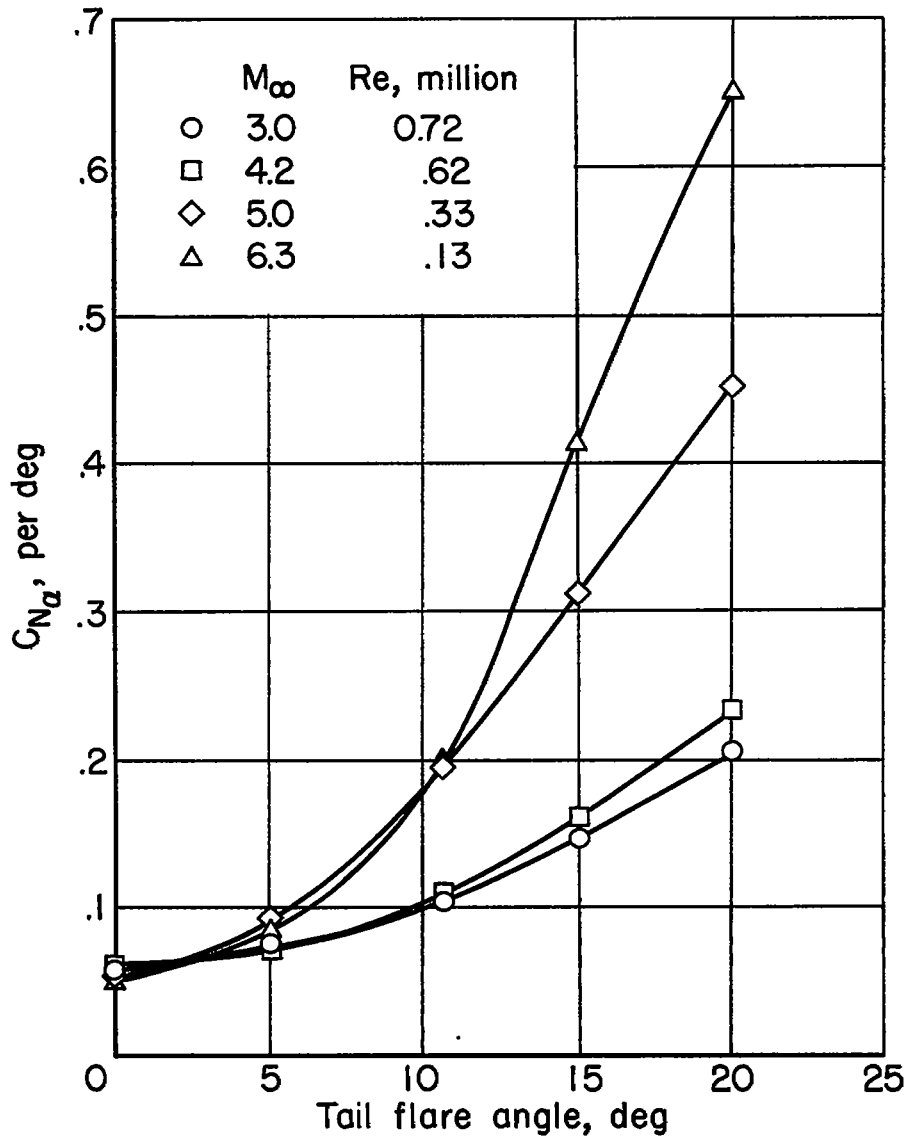
~~CONFIDENTIAL~~



(b) Bodies with fineness ratio 3 conical noses.

Figure 7.- Continued.

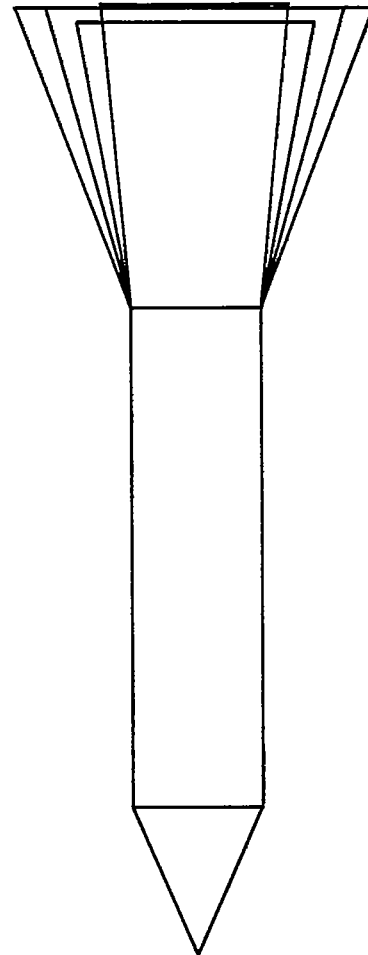
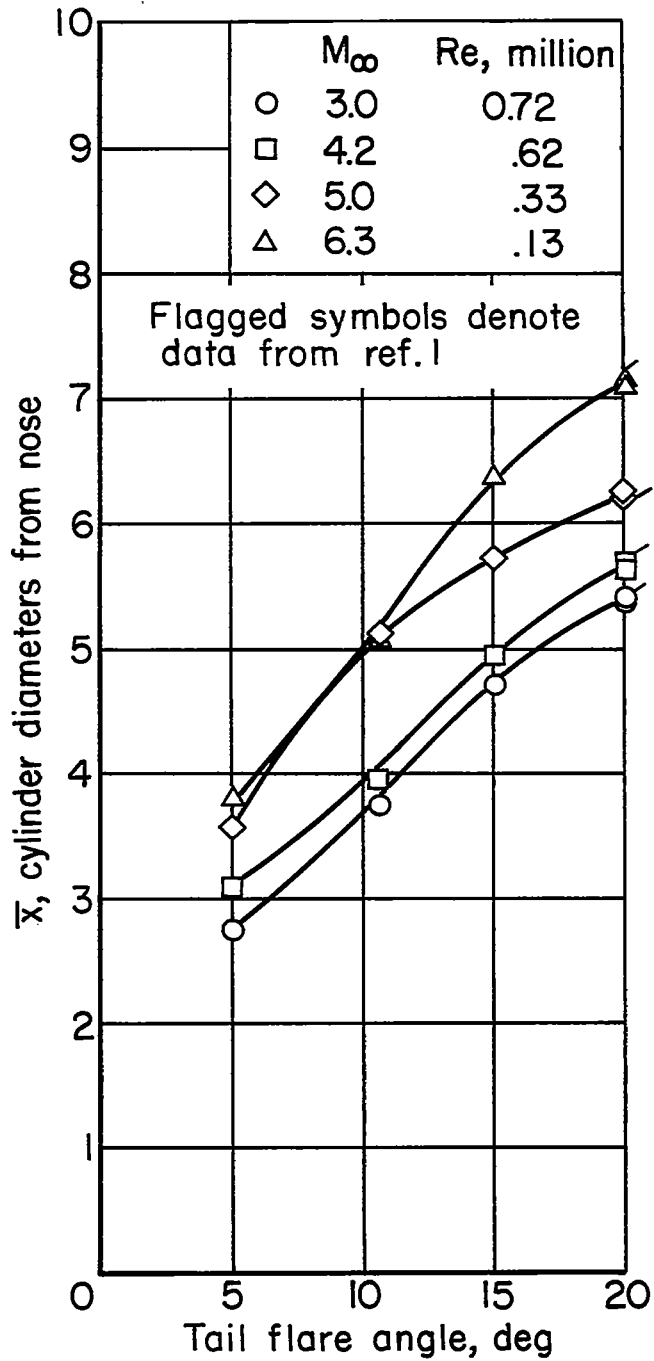
CONFIDENTIAL



(c) Bodies with fineness ratio 3 ogival noses.

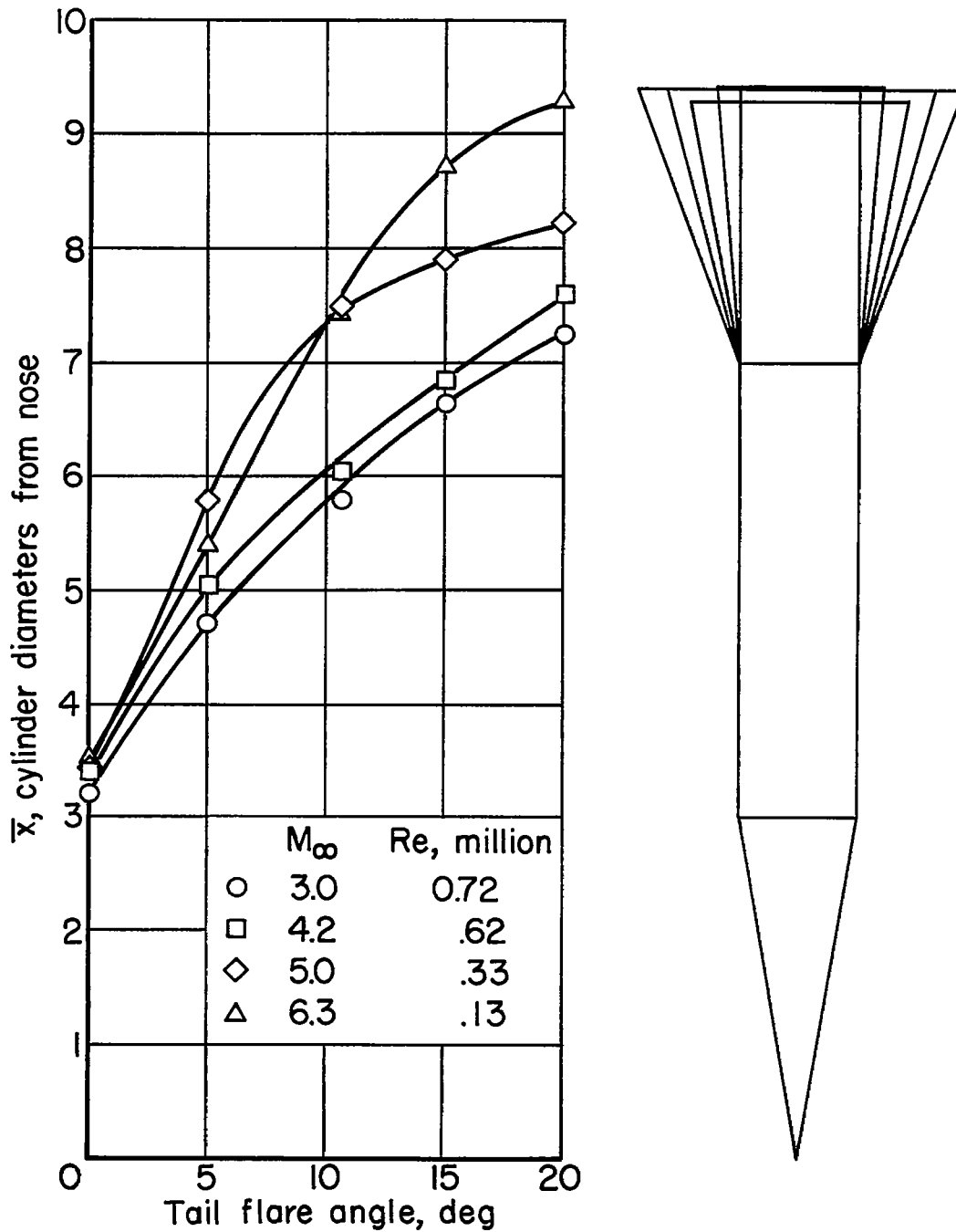
Figure 7.- Concluded.

CONFIDENTIAL



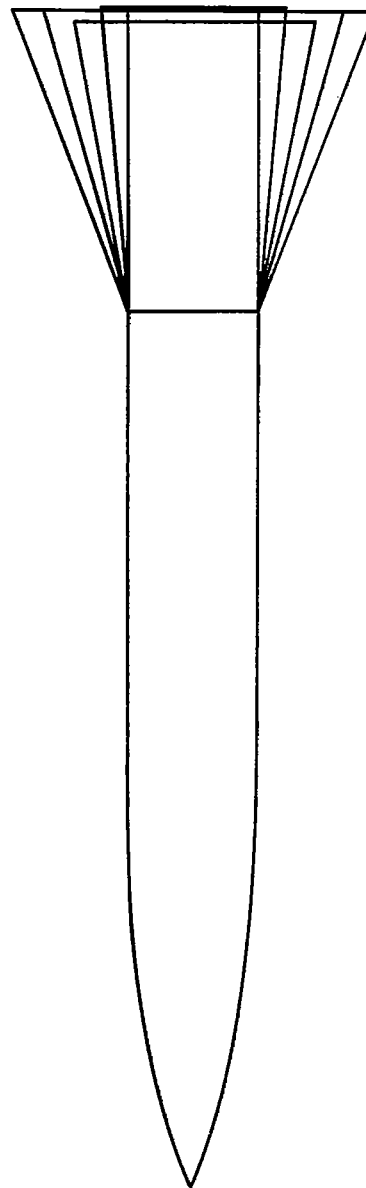
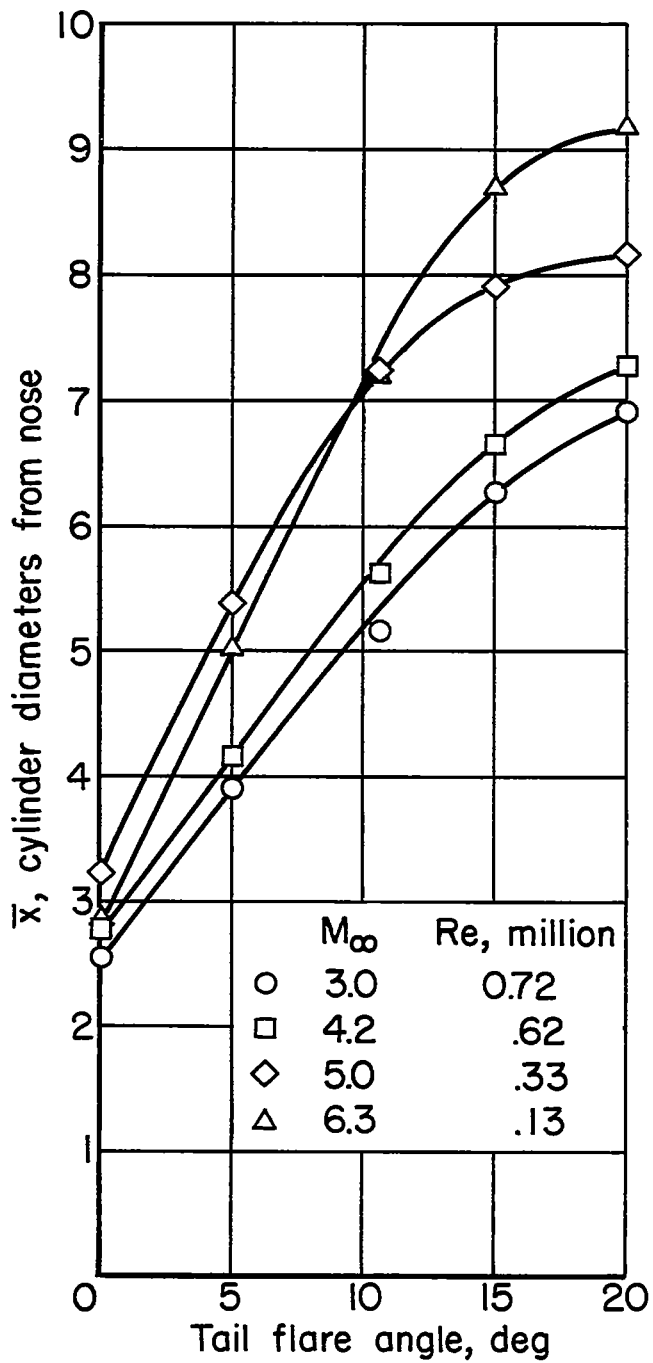
(a) Bodies with fineness ratio 1.2 conical noses.

Figure 8.- Variations of center-of-pressure positions with tail flare angle for the 12 test bodies.



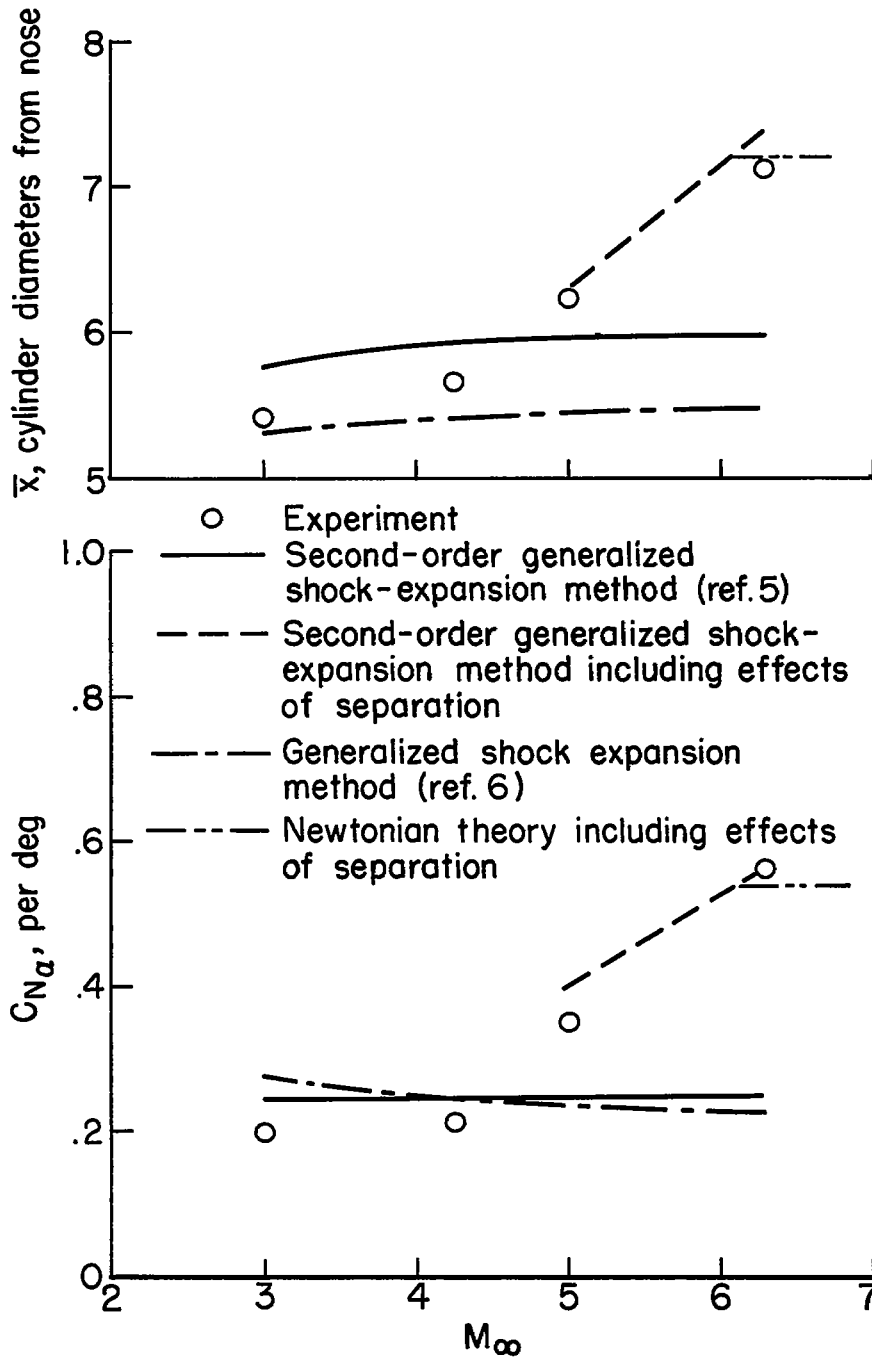
(b) Bodies with fineness ratio 3 conical noses.

Figure 8.- Continued.



(c) Bodies with fineness ratio 3 ogival noses

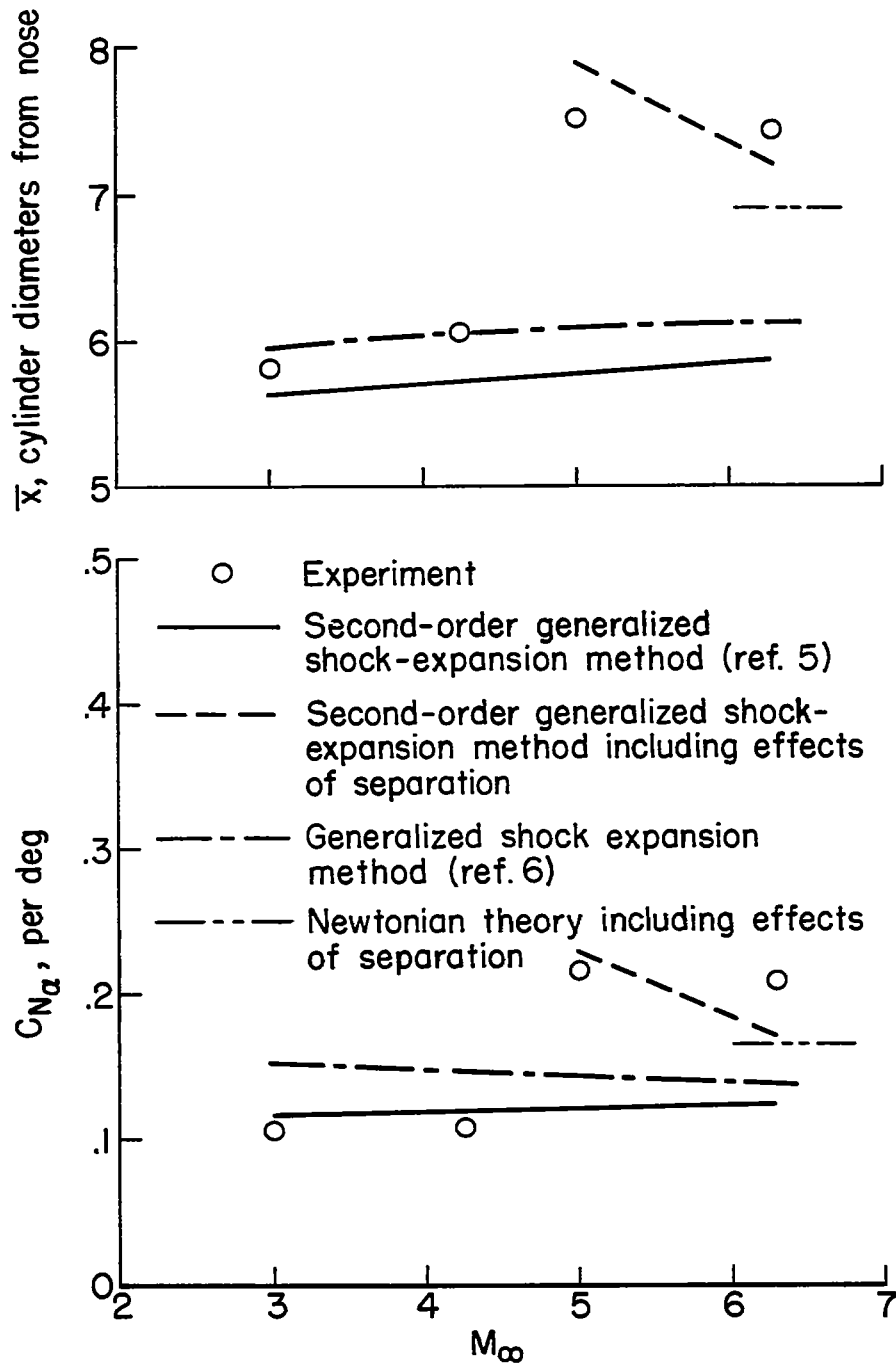
Figure 8.- Concluded.

~~CONFIDENTIAL~~

(a) Test body with fineness ratio 1.2 conical nose and 20° tail flare.

Figure 9.- Comparisons of theoretical results for center-of-pressure position and normal-force-curve slope with experimental results.

~~CONFIDENTIAL~~



(b) Test body with fineness ratio 3 conical nose and 10.5° tail flare.

Figure 9.- Concluded.